NREL
NATIONAL RENEWABLE ENERGY LABORATORY

# Feasibility Studies on Disturbance Feedforward Techniques to Improve Load Mitigation Performance

## January 2009 — January 2010

J.H. Laks, F. Dunne, and L.Y. Pao
*University of Colorado*
*Boulder, Colorado*

**NREL is a national laboratory of the U.S. Department of Energy, Office of Energy Efficiency & Renewable Energy, operated by the Alliance for Sustainable Energy, LLC.**

**Subcontract Report**
NREL/SR-5000-48598
December 2010

Contract No. DE-AC36-08GO28308

NREL
NATIONAL RENEWABLE ENERGY LABORATORY

# Feasibility Studies on Disturbance Feedforward Techniques to Improve Load Mitigation Performance

## January 2009 — January 2010

J.H. Laks, F. Dunne, and L.Y. Pao
*University of Colorado*
*Boulder, Colorado*

NREL Technical Monitor: Alan Wright

Prepared under Subcontract No. XEE-9-99404-01



National Renewable Energy Laboratory
1617 Cole Boulevard
Golden, Colorado 80401
303-275-3000 • www.nrel.gov

**Subcontract Report**
NREL/SR-5000-48598
December 2010

Contract No. DE-AC36-08GO28308

**This publication received minimal editorial review at NREL.**



Available electronically at http://www.osti.gov/bridge

Available for a processing fee to U.S. Department of Energy
and its contractors, in paper, from:

U.S. Department of Energy
Office of Scientific and Technical Information

P.O. Box 62
Oak Ridge, TN 37831-0062
phone: 865.576.8401
fax: 865.576.5728
email: mailto:reports@adonis.osti.gov

Available for sale to the public, in paper, from:

U.S. Department of Commerce
National Technical Information Service
5285 Port Royal Road
Springfield, VA 22161
phone: 800.553.6847
fax: 703.605.6900
email: orders@ntis.fedworld.gov
online ordering: http://www.ntis.gov/help/ordermethods.aspx

Cover Photos: (left to right) PIX 16416, PIX 17423, PIX 16560, PIX 17613, PIX 17436, PIX 17721

Printed on paper containing at least 50% wastepaper, including 10% post consumer waste.

# Feasibility Studies on Disturbance Feedforward Techniques to Improve Load Mitigation Performance *†

J.H. Laks, F. Dunne, and L.Y. Pao

**Abstract**

Light detection and ranging systems can measure conditions at a distance in front of wind turbines, and therefore are well suited to providing preview information of wind disturbances before they impact the turbine blades. As such, this technology makes available measurements of wind speed for use in disturbance feedforward control techniques. This study investigates disturbance feedforward and preview control to better understand the best possible improvement in load mitigation using advanced wind measurement techniques.

*The work reported here also is financially supported by industry partners.

†The authors thank Kathryn Johnson and Na Wang from the Colorado School of Mines for results in which feedforward control has been further augmented with additional feedback to enhance damping.

# List of Acronyms, Abbreviations, and Nomenclature

| | |
|---|---|
| $1P$ | once per rotor revolution |
| amp | amplitude |
| AR | above rated wind speeds |
| $A$ | average matrix of state-to-state coefficients for the turbine/pitch actuator model |
| $A(\theta)$ | matrix of state-to-state coefficients for the turbine/pitch actuator model at each rotor azimuth |
| $A_{1p}$ | state-to-state matrix of coefficients for parallel $1P$ harmonic oscillators |
| $A_{ar}$ | matrix of state-to-state coefficients for the pitch actuator model |
| $A_{dt}$ | state-to-state matrix of coefficients for weighting dynamics penalizing drivetrain |
| $A_{MBC}$ | average MBC matrix of state-to-state coefficients for the turbine/pitch actuator model |
| $A_{MBC}(\theta)$ | MBC matrix of state-to-state coefficients for the turbine/pitch actuator model at each rotor azimuth |
| $A_{sys}$ | average matrix of state-to-state coefficients for the turbine/actuator/measure-delay model |
| $A_D$ | state-to-state matrix of coefficients of wind-measurement delay chain |
| $A_F(\theta)$ | matrix of state-to-state coefficients from the FAST linearization at each rotor azimuth |
| B-Local | blade local |
| $b_{1,2,3}$ | blade-root bending moments in the flap direction for blades 1, 2, 3 |
| $B_{1p}$ | input-to-state matrix of coefficients for parallel $1P$ harmonic oscillators |
| $B_{ap}$ | matrix of command-to-state coefficients for the pitch actuator model |
| $B_{dt}$ | input-to-state matrix of coefficients for weighting dynamics penalizing drivetrain |
| $B_{F\beta}(\theta)$ | matrix of pitch-to-state coefficients from the FAST linearization at each rotor azimuth |
| $B_{Fsh}(\theta)$ | matrix of wind-to-state coefficients from the FAST linearization at each rotor azimuth |
| $B_{pMBC}$ | average MBC matrix of pitch-to-state coefficients for the turbine/pitch actuator model |
| $B_{pMBC}(\theta)$ | MBC matrix of pitch-to-state coefficients for the turbine/pitch actuator model at each rotor azimuth |
| $b_{rnr}$ | MBC/non-rotating component vector of blade-root bending moments [kN-m] in the flap direction |
| $B_{sh}(\theta)$ | matrix of FAST wind-to-state coefficients for the turbine/pitch actuator model at each rotor azimuth |
| $B_{sysp}$ | average matrix of pitch-to-state coefficients for the turbine/actuator/measure-delay model |
| $B_{sysw}$ | average matrix of B-local wind-to-state coefficients for the turbine/actuator/measure-delay model |
| $B_w(\theta)$ | matrix of B-local wind-to-state coefficients for the turbine/pitch actuator model at each rotor azimuth |
| $B_{wMBC}$ | average MBC matrix of B-local wind-to-state coefficients for the turbine/pitch actuator model |
| $B_{wMBC}(\theta)$ | MBC matrix of B-local wind-to-state coefficients for the turbine/pitch actuator model at each rotor azimuth |
| $B_C$ | MBC cosine/vertical component of blade flap moments |
| $B_D$ | input-to-state matrix of coefficients of wind-measurement delay chain |

| | |
|---|---|
| $B_p$ | average matrix of pitch-to-state coefficients for the turbine/pitch actuator model |
| $B_p(\theta)$ | matrix of pitch-to-state coefficients for the turbine/pitch actuator model at each rotor azimuth |
| $b_r$ | vector of blade-root bending moments [kN-m] in the flap direction |
| $B_S$ | MBC sine/horizontal component of blade flap moments |
| $B_U$ | MBC uniform/collective component of blade flap moments |
| $B_w$ | average matrix of B-local wind-to-state coefficients for the turbine/pitch actuator model |
| CART3 | 3-bladed controls advanced research turbine |
| CP | collective pitch |
| CRUNCH | NWTC software for wind turbine data analysis |
| $\begin{bmatrix} C_{1ps} \\ C_{1pc} \end{bmatrix}$ | state-to-output matrix of coefficients for parallel $1P$ harmonic oscillators |
| $C_\beta$ | pitch controller for rotor speed |
| $C_{\beta h}$ | pitch controller for MBC horizontal component |
| $C_{\beta v}$ | pitch controller for MBC vertical component |
| $C_{ap}$ | matrix of state-to-pitch coefficients for the pitch actuator model |
| $C_{apr}$ | matrix of state-to-pitch rate coefficients for the pitch actuator model |
| $C_{bMBC}$ | average MBC matrix of state-to-bend moment coefficients for the turbine/pitch actuator model |
| $C_{bMBC}(\theta)$ | MBC matrix of state-to-bend moment coefficients for the turbine/pitch actuator model at each rotor azimuth |
| $C_{dt}$ | state-to-output matrix of coefficients for weighting dynamics penalizing drivetrain |
| $C_{Fb}(\theta)$ | matrix of state-to-bend moment coefficients from the FAST linearization at each rotor azimuth |
| $C_{Fg}(\theta)$ | matrix of state-to-generator-speed coefficients from the FAST linearization at each rotor azimuth |
| $C_{gMBC}(\theta)$ | MBC matrix of state-to-generator-speed coefficients for the turbine/pitch actuator model at each rotor azimuth |
| $C_{rMBC}$ | average MBC matrix of state-to-pitch rate coefficients for the turbine/pitch actuator model |
| $C_{rMBC}(\theta)$ | MBC matrix of state-to-pitch rate coefficients for the turbine/pitch actuator model at each rotor azimuth |
| $C_{sway}$ | pitch controller for tower sway |
| $C_{sysb}$ | average matrix of state-to-bend moment coefficients for the turbine/actuator/measure-delay model |
| $C_{sysr}$ | average matrix of state-to-pitch rate coefficients for the turbine/actuator/measure-delay model |
| $C_b$ | average matrix of state-to-bend moment coefficients for the turbine/pitch actuator model |
| $C_b(\theta)$ | matrix of state-to-bend moment coefficients for the turbine/pitch actuator model at each rotor azimuth |
| $C_D$ | state-to-output matrix of coefficients of wind-measurement delay chain |
| $C_g(\theta)$ | matrix of state-to-generator-speed coefficients for the turbine/pitch actuator model at each rotor azimuth |
| $C_r$ | average matrix of state-to-pitch rate coefficients for the turbine/pitch actuator model |
| $C_r(\theta)$ | matrix of state-to-pitch rate coefficients for the turbine/pitch actuator model at each rotor azimuth |

| | |
|---|---|
| dB/dec | decibels per decade |
| DEL | damage equivalent load |
| DOF | degree of freedom |
| $D_{ap}$ | matrix of command-to-pitch coefficients for the pitch actuator model |
| $D_{apr}$ | matrix of command-to-pitch rate coefficients for the pitch actuator model |
| $D_{bp}$ | average matrix of pitch-to-bend moment coefficients for the turbine/pitch actuator model |
| $D_{bp}(\theta)$ | matrix of pitch-to-bend moment coefficients for the turbine/pitch actuator model at each rotor azimuth |
| $D_{bpMBC}$ | average MBC matrix of pitch-to-bend moment coefficients for the turbine/pitch actuator model |
| $D_{bpMBC}(\theta)$ | MBC matrix of pitch-to-bend moment coefficients for the turbine/pitch actuator model at each rotor azimuth |
| $D_{bsh}(\theta)$ | matrix of FAST wind-to-bend moment coefficients for the turbine/pitch actuator model at each rotor azimuth |
| $D_{bw}$ | average matrix of B-local wind-to-bend moment coefficients for the turbine/pitch actuator model |
| $D_{bw}(\theta)$ | matrix of B-local wind-to-bend moment coefficients for the turbine/pitch actuator model at each rotor azimuth |
| $D_{bwMBC}$ | average MBC matrix of B-local wind-to-bend moment coefficients for the turbine/pitch actuator model |
| $D_{bwMBC}(\theta)$ | MBC matrix of B-local wind-to-bend moment coefficients for the turbine/pitch actuator model at each rotor azimuth |
| $D_{Fbp}(\theta)$ | matrix of pitch-to-bend moment coefficients from the FAST linearization at each rotor azimuth |
| $D_{Fbsh}(\theta)$ | matrix of wind-to-bend moment coefficients from the FAST linearization at each rotor azimuth |
| $D_{Fgp}(\theta)$ | matrix of pitch-to-generator-speed coefficients from the FAST linearization at each rotor azimuth |
| $D_{Fgsh}(\theta)$ | matrix of wind-to-generator-speed coefficients from the FAST linearization at each rotor azimuth |
| $D_{gp}(\theta)$ | matrix of pitch-to-generator-speed coefficients for the turbine/pitch actuator model at each rotor azimuth |
| $D_{gpMBC}(\theta)$ | MBC matrix of pitch-to-generator-speed coefficients for the turbine/pitch actuator model at each rotor azimuth |
| $D_{gsh}(\theta)$ | matrix of FAST wind-to-generator-speed coefficients for the turbine/pitch actuator model at each rotor azimuth |
| $D_{gw}(\theta)$ | matrix of B-local wind-to-generator-speed coefficients for the turbine/pitch actuator model at each rotor azimuth |
| $D_{gwMBC}(\theta)$ | MBC matrix of B-local wind-to-generator-speed coefficients for the turbine/pitch actuator model at each rotor azimuth |
| $D_{rp}$ | average matrix of pitch-to-pitch rate coefficients for the turbine/pitch actuator model |
| $D_{rp}(\theta)$ | matrix of pitch-to-pitch rate coefficients for the turbine/pitch actuator model at each rotor azimuth |
| $D_{rpMBC}$ | average MBC matrix of pitch-to-pitch rate coefficients for the turbine/pitch actuator model |
| $D_{rpMBC}(\theta)$ | MBC matrix of pitch-to-pitch rate coefficients for the turbine/pitch actuator model at each rotor azimuth |

| | |
|---|---|
| $D_{rsh}(\theta)$ | matrix of FAST wind-to-pitch rate coefficients for the turbine/pitch actuator model at each rotor azimuth |
| $D_{rw}$ | average matrix of B-local wind-to-pitch rate coefficients for the turbine/pitch actuator model |
| $D_{rw}(\theta)$ | matrix of B-local wind-to-pitch rate coefficients for the turbine/pitch actuator model at each rotor azimuth |
| $D_{rwMBC}$ | average MBC matrix of B-local wind-to-pitch rate coefficients for the turbine/pitch actuator model |
| $D_{rwMBC}(\theta)$ | MBC matrix of B-local wind-to-pitch rate coefficients for the turbine/pitch actuator model at each rotor azimuth |
| $D_{sysbp}$ | average matrix of pitch-to-bend moment coefficients for the turbine/actuator/measure-delay model |
| $D_{sysbw}$ | average matrix of B-local wind-to-bend moment coefficients for the turbine/actuator/measure-delay model |
| $D_{sysrp}$ | average matrix of pitch-to-pitch rate coefficients for the turbine/actuator/measure-delay model |
| $D_{sysrw}$ | average matrix of B-local wind-to-pitch rate coefficients for the turbine/actuator/measure-delay model |
| FA | fore-aft |
| FAST | NWTC aeroelastic design code for horizontal axis wind turbines |
| FF | feedforward |
| FIR | finite impulse response |
| GP-LLJ | Great Plains low level jet |
| IP | individual pitch |
| kW | kilowatt |
| LIDAR | light detection and ranging |
| LIFE2 | computer code for wind turbine fatigue analysis |
| LMI | linear matrix inequality |
| m | meter |
| MBC | multi-blade coordinate transformation |
| MIMO | multiple-input multiple-output |
| MW | megawatt |
| $M_{m2sh}$ | matrix of coefficients to scale from FAST wind-shear perturbations to MBC wind perturbations |
| Nm | Newton-meters |
| NPZ-Ignore | nonminimum-phase zeros ignore |
| NREL | National Renewable Energy Laboratory |
| NWTC | National Wind Technology Center |
| PI | proportional-integral |
| $p$ | vector of pitch-command inputs [rad] to the actuators |
| $p_{1,2,3}$ | pitch commands [rad] for the three blades |
| $p_{nr}$ | MBC/non-rotating component vector of pitch [rad] command to the actuators |
| $P_C$ | MBC pitch-command cosine/vertical component |
| $P_S$ | MBC pitch-command sine/horizontal component |
| $P_U$ | MBC pitch-command uniform/collective component |
| R | near rated wind speeds |
| rad | radians |
| rms | root mean square |

| | |
|---|---|
| rpm | revolutions per minute |
| $R$ | nominal blade radius [m] |
| $r_0$ | radius [m] at which individual wind measurements are made |
| $Ri_{TL}$ | vertical stability parameter |
| s | second |
| SDPT3 | Matlab® software for semidefinite-quadratic-linear programming |
| SISO | single-input single-output |
| SS | side to side |
| $T(\theta)$ | inverse MBC transformation matrix (a function of rotor azimuth) |
| $u_{*_D}$ | mean friction velocity (shearing stress) |
| $v_r$ | velocities [m/s] corresponding to $x_r$ |
| w | vector of individual wind measurements [m/s], one per blade |
| $\mathrm{w}_{1,2,3}$ | wind speeds [m/s] at the three blades |
| $\mathrm{w}_{mbc}$ | vector of wind measurement MBC components (uniform, cosine, sine) [m/s] |
| $\mathrm{w}_{sh}$ | vector of fixed-frame wind perturbations used by FAST for linearization |
| $\mathrm{w}_{ti}$ | present wind speed [m/s] at each turbine blade $i$ $(= 1, 2, 3)$ |
| $\mathrm{w}_0$ | average (across the rotor disk) wind speed [m/s] |
| $\mathrm{w}_t$ | vector of all three wind speeds $w_{ti}$ presently at turbine blades |
| $x_{ar}$ | vector of pitch actuator angles/states [rad] |
| $x_W$ | vector of wind speeds $x_{wi}$ approaching all blades |
| $x_{wi}$ | discrete time sampled wind speeds [m/s] approaching blade $i$ $(= 1, 2, 3)$ |
| $x_r$ | displacements [m] that are inherently part of the blades |
| $x_t$ | vector of all other (fixed reference frame) turbine states |
| YALMIP | Matlab® toolbox for modeling and solving optimization problems |
| ZMETC | zero magnitude error tracking controller |
| ZPETC | zero phase error tracking controller |
| $\alpha_D$ | vertical wind shear power law exponent |
| $\beta$ | vector of pitch angles [rad] achieved by the actuators |
| $\beta_{rnr}$ | vector of MBC/non-rotating pitch-rate [rad/sec] components produced by the pitch actuators |
| $\beta_r$ | vector of pitch rates [rad/sec] produced by the pitch actuators |
| $\Omega$ | rotor speed [rad/sec] |
| $\omega_{1p}$ | once per rotor revolution in [rad/second] |
| $\Omega_g$ | generator speed [rpm] |
| $\tau_{prev}$ | time delay [sec] between preview measurements of wind speed and wind arrival at the turbine |
| $\theta$ | rotor azimuth [rad]; the clockwise angle of blade 1 from upward vertical |
| $\theta_{prev}$ | expected angle [rad] of blade 1 after the elapsed preview time |

# Contents

# List of Figures

# List of Tables

# Executive Summary

## 0.1 Background

The objective of this phase 1 feasibility study is to investigate improvements in blade and tower load mitigation by using disturbance feedforward and feedback control techniques based on wind measurements as might be obtained with light detection and ranging (LIDAR) systems. The various feedback and feedforward controllers studied are designed for the National Renewable Energy Laboratory's (NREL) model of a 5-MW turbine (Jonkman et al. [1]) as well as a model of NREL's 3-Bladed Controls Advanced Research Turbine (CART3). Variations of collective-pitch control (a subset of the controllers studied) are shown in Figure 0.1. Disturbance feedforward and preview techniques utilize measurements of the disturbance (in this case wind) as shown in Figure 0.1(b) and 0.1(c), and feedback-only control is used in (a).

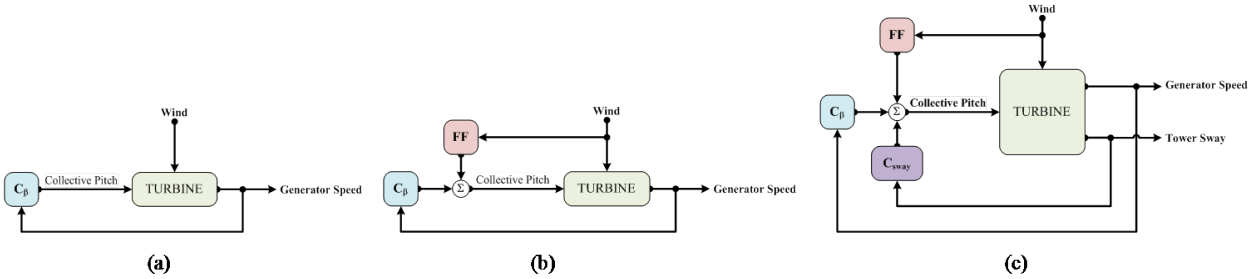


Figure 0.1. collective-pitch control configurations: (a) feedback only, (b) feedback augmented with disturbance feedforward, (c) feedforward with multiple single-input-single-output feedback loops to address different objectives

The 5-MW study is the first research on feedforward conducted by this team for that turbine model and the CART3 study is the second study of this type in applying disturbance feedforward. As such, the 5-MW turbine studies examine augmenting typical industry feedback control with disturbance feedforward controllers, and the CART3 controllers investigated are more advanced and further removed from those typically used in industry.

These investigations are conducted through simulation of the turbine models using FAST (Jonkman et al. [2]) within the Mathworks Simulink® block-diagram environment as depicted in Figure 0.2. Full-field descriptions of the instantaneous wind conditions used during simulations are generated using TurbSim (Kelly et al. [3]); the resulting wind files are accessed automatically by the FAST code and the controllers and other blocks are implemented in Simulink®.

So that the controllers have access to wind speeds for use in feedforward compensation, the FAST code is modified to provide wind speeds at desired measurement locations. When the measurement locations are upwind from the turbine, the wind speeds obtained are referred to as "preview." Preview measurements provide information to the feedforward compensation before the previewed wind speeds impact the turbine; LIDAR is well suited to provide this type of data because it is more easily configured to take measurements ahead of the turbine rather than directly at the turbine blades.

An earlier study (Laks et al. [5]) on the CART3 examined using disturbance feedforward techniques

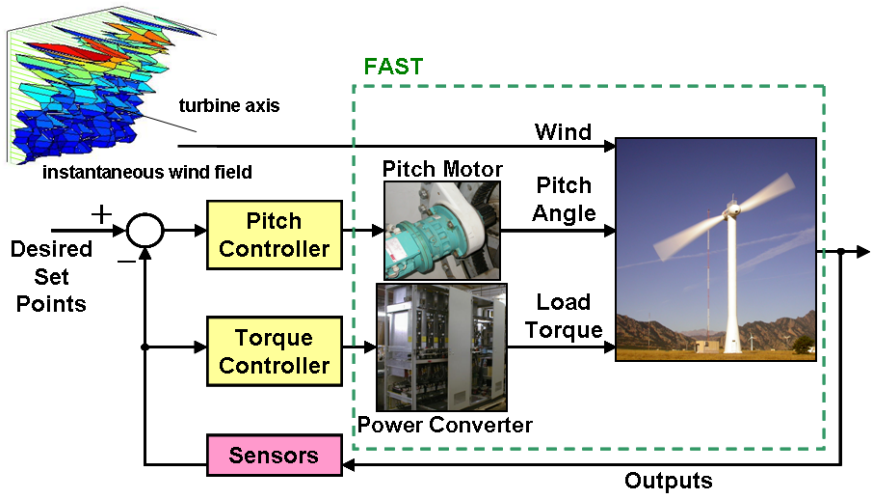


Figure 0.2. Wind turbine feedback-control block diagram (modified from Pao and Johnson 2009 [4] with permission)

without the benefit of preview and found that it was not possible to improve performance without excessive pitch rates. Therefore, in this second study for the CART3, only feedforward with preview is investigated further. The 5-MW studies look at using disturbance feedforward techniques both with and without the use of preview measurements. As a result, there is a greater number of 5-MW controller variations than for the CART3 studies, as summarized in Table 0.1. The controller numbers in Table 0.1 are used to identify the controllers throughout the report.

Two levels of baseline control are designed for both the 5-MW turbine and the CART3. The most basic is a collective pitch (CP) based on feedback of the generator-speed error to regulate speed. The second baseline controller augments the CP loop with feedback from the vertical and horizontal components of the blade-root bending moment to obtain baseline individual-pitch controllers (Bossanyi [6]). As summarized in Table 0.1, permutations of the 5-MW controllers are distinguished by combining the single-input-single-output (SISO) baseline loops with additional feedforward controllers or tower and blade feedback controllers, and also by whether the pitch command is collective or independent. Permutations of the CART3 controllers, also summarized in Table 0.1, are distinguished by the use of a single multi-input-multi-output (MIMO) controller, and by whether these MIMO controllers are based on multi-blade coordinates (MBC) (Bir [7]) or individual, blade-local (B-Local) measurements and pitch commands.

## 0.2 Procedure

During simulation, the FAST code reads the wind field files generated by TurbSim and uses aero-elastic computations to determine the loads on and interaction with the turbine blades and tower. In the case of the 5-MW turbine, the wind-field parameters are based on extensive observations taken in the high-plains environment of southeast Colorado. The Great Plains (GP-LLJ) spectral model available in TurbSim was used to simulate wind conditions present at this site. In the case of the CART3, wind-field parameters are based on conditions representative of the National Wind Technology Center (NWTC) in Golden, Colorado, where it is located. As summarized in Table 0.2, wind fields for the 5-MW turbine are generated at near-rated (R) and above-rated (AR) conditions

Table 0.1. A Sample of the Controller Configurations Explored in this Feasibility Study; the 5-MW Controllers are Industry Standard Control Augmented with Feedforward; the CART3 Feedforward Controller Variations are Single, MIMO Loops and so the Only Permutations are Distinguished by the Use of MBC; Controllers 4 and 5 are Tower Damping and Tower and Blade Damping Augmentations; these Controllers were Studied Under a Separate but Related Industry Funded Project; the Details of These Controllers are Documented in Laks et al. [8].

| Turbine | Cont roller | Description (signals used) |
|---|---|---|
| 5-MW | (1) | Collective pitch baseline (generator speed) |
| | (2) | (1) Plus individual pitch feedback (generator speed, blade-flap moments) |
| | (3) | (1) Plus individual pitch feedforward (generator speed, 10/3 s wind preview at each blade) |
| | (4) | (3) Plus tower damping feedback (generator speed, 10/3 s wind preview at each blade, fore-aft tower velocity) |
| | (5) | (3) Plus tower and blade damping feedback (generator speed, 10/3 s wind preview at each blade, fore-aft tower and blade-tip velocities and deflections) |
| | | |
| CART3 (675 kW) | (6) | Collective pitch baseline (generator speed) |
| | (7) | (6) Plus individual pitch feedback (generator speed, blade-flap moments) |
| | (8) | MIMO individual pitch (generator speed, blade-flap moments, 0.45 s wind preview at each blade) |
| | (9) | MIMO MBC individual pitch (generator speed, blade-flap moments, 0.45 s wind preview at each blade) |

as determined by average hub-height horizontal wind speed. The CART3 studies only focused on load mitigation in AR conditions. By focusing on above-rated conditions, the load mitigation performance is kept separate from other considerations that come into play in near-rated conditions where the turbine could continually transition between Region 2 (below rated operating scheme) and Region 3 (above rated operating scheme). Three different wind conditions are generated for the R and AR cases and are distinguished by atmospheric boundary characteristics.

In each of the ensembles of the wind-speed categories, 31 realizations of the turbulent wind field based on the specified boundary conditions are generated. Each controller configuration for the 5-MW and CART3 turbine model is simulated in all of the resulting wind fields. Loads and other turbine variables of interest are stored and then post-processed after simulation to compute performance metrics.

Wind measurements used for feedforward control can be divided roughly into two categories. The exact method used in each case is discussed in Section 3. Essentially, the main difference is whether the measurement locations rotate in coordination with the blades or the locations remain stationary. In the former case, wind measurements are used for IP feedforward compensation. In the latter

Table 0.2. Turbulence Boundary Conditions Used to Generate Wind Fields; Each of the 3 Wind Speed Categories are Varied by the Vertical Stability Parameter $Ri_{TL}$ and the Mean Friction Velocity (Shearing Stress) $u_{*_D}$ Over the Rotor Disk; a Power Law Variation of the Vertical Wind Speed Profile is Specified by the Listed Shear Exponents $\alpha_D$

| Turbine | | Ensemble | Mean Wind [m/s] | $Ri_{TL}$ | $\alpha_0$ | $U_{*_D}$ [m/s] |
|---|---|---|---|---|---|---|
| 5 MW | Near Rated | R1 | 11.4 | -0.100 | 0.086 | 0.451 |
| | | R2 | 11.4 | 0.020 | 0.134 | 0.414 |
| | | R3 | 11.4 | 0.200 | 0.365 | 0.149 |
| | Above Rated | AR1 | 13 | -0.100 | 0.077 | 0.514 |
| | | AR2 | 13 | 0.020 | 0.139 | 0.422 |
| | | AR3 | 13 | 0.200 | 0.363 | 0.135 |
| CART3 | Above Rated | AR4 | 18 | -0.180 | 0.110 | 0.682 |
| | | AR5 | 18 | 0.021 | 0.134 | 0.860 |
| | | AR6 | 18 | 0.043 | 0.125 | 0.688 |

case, the measurements are averaged to provide CP feedforward control, or the stationary measurements are interpolated to estimate wind speeds at rotating locations for use in stationary-based IP feedforward.

The torque controller for both the 5-MW and the CART3 is a non-dynamic computation based on rotor speed. Both the 5-MW and CART3 controllers use a standard square law (Jonkman et al. [1]) when the rotor speed drops into Region 2 (below rated conditions). In Region 3 (wind speeds above rated conditions), the 5-MW torque controller adjusts torque to maintain rated power but the CART3 controller holds torque constant.

## 0.3 Summary of Results

This section summarizes a few key simulation results in AR conditions with respect to mitigation of blade and tower loads. Results in R conditions are similar, and more detailed results are presented in the sections covering the respective turbine studies.

Results are computed in terms of the ensemble damage equivalent load (DEL) averaged over all simulations. That is, a DEL is computed for each AR simulation as distinguished by the controller and wind-measurement method. The DEL metric itself is calculated using the blade-root flap or tower base fore-aft bending moment observed during the simulation and is based on a rain-flow counting algorithm using code from NREL. This computation uses a Wohler curve exponent (slope of log(S) versus log(N), where S is the magnitude of a cyclical stress and N is the number of cycles to material failure) of 10, which is typical for composite materials. Each permutation of controller and wind-measurement scheme is simulated in all of the 93 AR wind realizations. The DEL is calculated for each simulation and the average then is taken over the resulting 93 metrics to determine the DEL performance for each control/measurement configuration.

Results representative of the 5-MW studies and those from the CART3 studies are shown in Figure 0.3 upper and lower plots, respectively. The studies show that preview measurements that give

information on wind speeds local to the blades provide an advantage over using feedback only. In both the 5-MW and CART3 studies, the CP baseline feedback-only results serve as a familiar reference point, representative of industry-standard control. The IP baseline feedback-only controllers are improved designs with lower DELs than CP. Results are normalized to give IP baseline DELs of 100, so the remaining individual-pitch preview controller DELs easily can be compared to the IP baseline. The IP baseline controllers provide significant load mitigation over that obtained with CP feedback-only control; and adding disturbance feedforward using blade-local (rotating) preview measurements can provide still further performance improvement.

## 0.4 Discussion and Future Work

We think that the difference between the 5-MW study and the CART3 study mainly is attributable to the fact that in the 5-MW study, the feedforward controllers are based on speed-regulation considerations. On the other hand, the CART3 MIMO preview approach is designed explicitly to reduce blade-root loads. It only is somewhat unexpected that the 5-MW feedforward based on speed regulation also provides load mitigation, because the technique utilized should have the effect of smoothing out the pitch response in the correct direction where feedback only would be "late" and potentially suffer greater transients. An additional difference between the two studies is that the preview time (0.45 s) used for the CART3 case now is known to be nearly optimal (see Figure 17 in Section 5.1) and the optimal amount of preview for the 5-MW still is a topic for further investigation.

Further, the fact that the more accurate measurement scheme rotates in unison with the blades is not the salient characteristic. Rather, it is the fact that the wind speed arriving local to each blade, after the elapsed preview time, is predicted accurately by the rotating measurements. We expect that any measurement scheme/LIDAR scanning pattern and signal processing algorithm that provides similar blade-local accuracy will have the same performance advantages.

In summary, we found that wind preview feedforward can be used to augment standard controllers to improve load mitigation, as in the 5-MW study. There are further advantages to a complete controller redesign, also using wind preview, as seen in the CART3 study. This can provide a 30% blade load reduction from baseline, while only a 10% blade load reduction was achieved in the 5-MW study before tower or blade damping was added. There are two important caveats in this regard, however. First, the 5-MW feedforward design methods could be based on load mitigation instead of speed regulation, and this should have a significant effect on the DEL performance. Second, the CART3 controllers developed so far are expensive in terms of computing resources, requiring easily more than 10 times the computation required for the baseline controllers (based on a comparison of the order of the controllers).

In the future a number of issues can be addressed using the same or slight modifications of techniques developed so far. Techniques applied to the CART3 can be applied to the 5-MW turbine, and a state-feedback study (as completed for the CART3) will also reveal the amount of preview required for "optimal" load mitigation on the 5-MW turbine. Moreover, we plan to incorporate the expected frequency content of wind perturbations into the control designs. We expect that doing so will provide better/more low-frequency emphasis and render benefits that are twofold. Wind perturbations tend to predominate at lower (below 1 Hz) frequencies, therefore emphasis at these frequencies should further improve performance. We also anticipate a decrease in sensitivity

to errors in wind measurements which appear to predominate at higher frequencies. Finally, it is possible to apply model order reduction techniques to the CART3 controllers to reduce the amount of computation these require. It remains to be seen whether the savings will be significant.

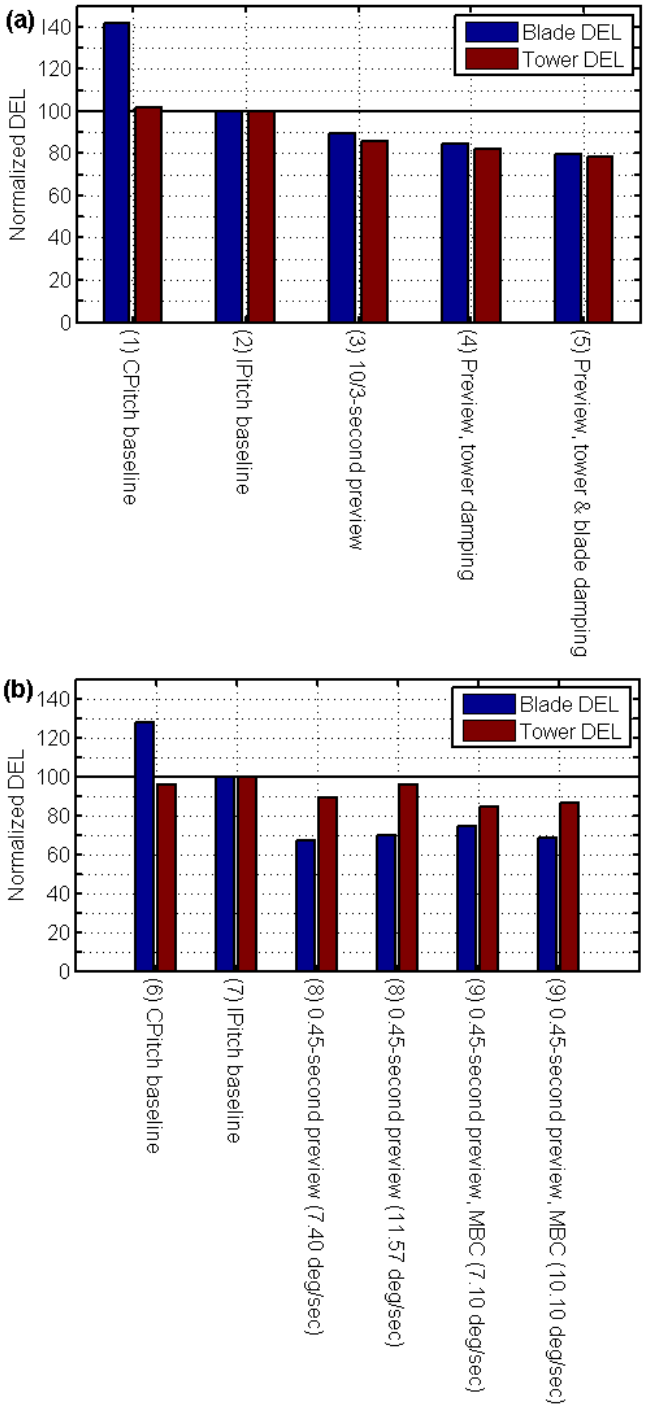


Figure 0.3. Blade-root flap and tower base damage equivalent loads for a sample of controllers studied (see Table 0.1 for a description of the controllers); results are normalized to an IP feedback-only baseline controller DEL of 100; a configuration producing a DEL lower than 100 has improved performance relative to IP baseline; the 5-MW results are shown in the upper plot (a), and the CART3 results are shown in (b); for the preview results presented here, 3 wind speed measurements, rotating with the blades, are taken at 75% span; in both cases, using preview feedforward based on measurements that accurately reflect conditions local to the blades provides advantages over feedback only

# 1 Introduction/Motivation

The stochastic nature of wind resources, the high initial capital cost, and the increasing structural flexibility of utility-scale turbines motivate the adoption of advanced instrumentation and measurement technologies. One of the most attractive technologies is LIDAR (light detection and ranging). It has the ability to make real-time measurements of wind conditions local to individual turbines. These types of measurements make it possible to employ disturbance feedforward techniques using a preview of actual wind speeds, instead of employing wind estimates obtained from measurements of the turbine structural dynamics (Ostergaard et al. [9]) which do not provide any preview.

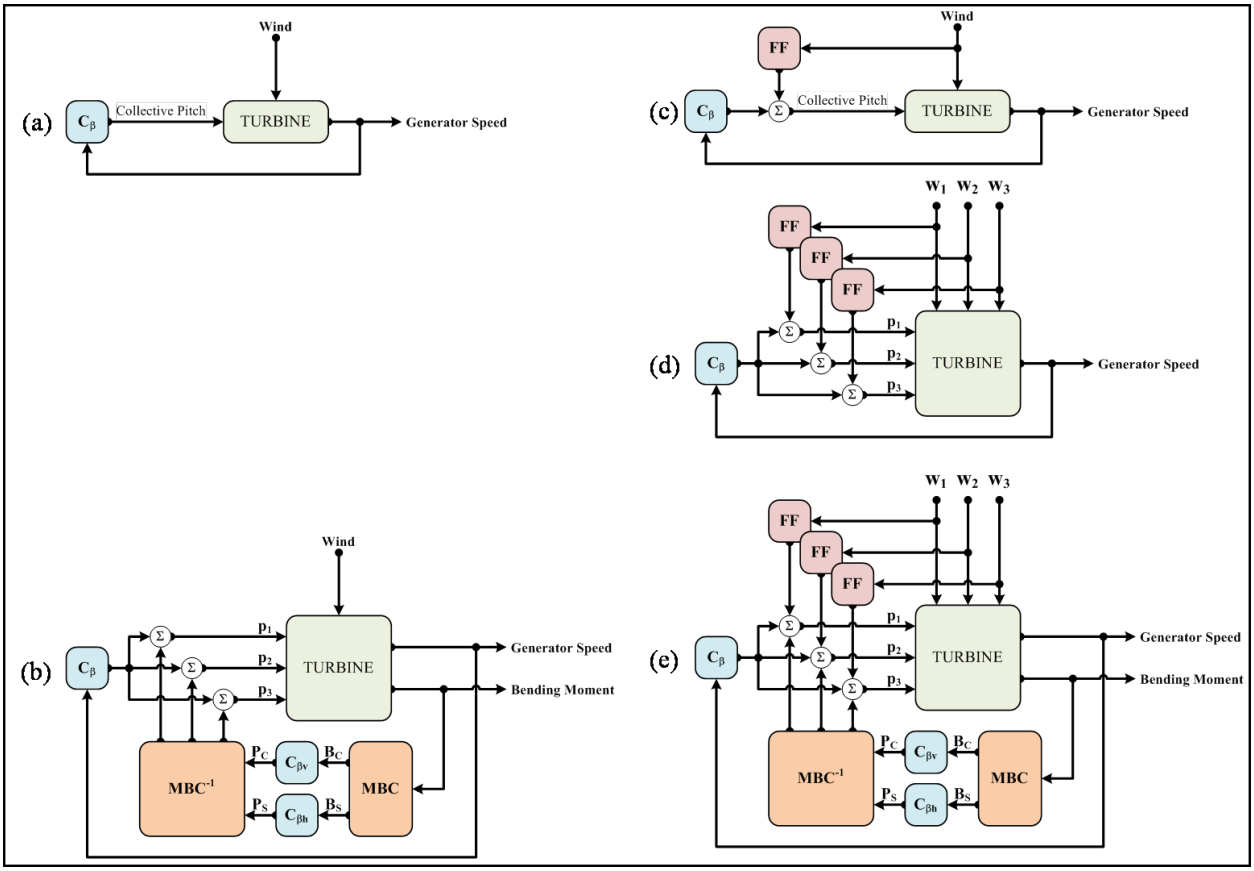


Figure 1. Feedforward SISO-based control schemes: (a) CP speed regulation; (b) CP + IP SISO loops; (c) CP, augmented with CP feedforward; (d) CP augmented with IP feedforward; (e) CP+IP SISO loops augmented with IP feedforward.

In this feasibility study, we attempt to better understand the best possible outcome that can be achieved with advanced measurement of wind speeds approaching the turbine. As this is an initial study, we focus on idealized measurements, which allows considerable simplification with respect to the configuration of the LIDAR than might otherwise be required (Schlipf et al. and Harris et al. [10, 11]).

Even with these simplifications, there still is a seemingly endless number of permutations of control schemes in which idealized measurements might be employed. Recent work by Bossanyi [6], Stol and Fingersh [12], Wright et al. [13], and Stol et al. [14] has verified that more advanced feed-

back controllers can reduce structural fatigue loads. These advanced controllers typically employ individual-pitch control and can be based on signals from strain gauges and position encoders in addition to generator speed. This study benchmarks disturbance feedforward techniques against some industry standard feedback control approaches. All of the controllers studied are simulated in turbulent wind conditions that have spatial variation beyond what would be produced by linear and vertical shear alone.

Standard feedback collective (CP) and independent (IP) pitch controllers, as depicted in Figure 1(a) and Figure 1(b), respectively, are designed for the 5-MW and CART3 turbines as baseline cases. The CP loop regulates turbine speed based on the generator-speed error. By adding to this CP-loop, the feedback from the vertical and horizontal components of the blade-root bending moment, a baseline IP controller is obtained.

The 5-MW studies focus on augmenting these baseline controllers with additional feedforward loops. Measurements of wind speed are fed forward as shown in Figure 1(c)–(e) to augment the standard feedback control. The CP baseline controller is augmented with both collective-pitch feedforward (Figure 1(c)) and IP feedforward (Figure 1(d)) and only IP feedforward (Figure 1(e)) is used to augment the IP baseline controller. The CP feedforward is based on stationary measurements used to compute a spatial average wind measurement and the IP feedforward uses measurements that rotate in unison with the blades.

With respect to the CART3, preview control is designed based on MIMO combined feedback and feedforward techniques as depicted in Figure 2. If there is significant interest in exploring the use of preview measures to augment existing controllers, a future study would be warranted. The variations in this study used for the CART3 controllers are based primarily on whether they make use of blade local variables (Figure 2(a)) or MBC coordinates (Figure 2(b)), with further gradations based on the rms pitch rate and the method used to measure wind speeds.

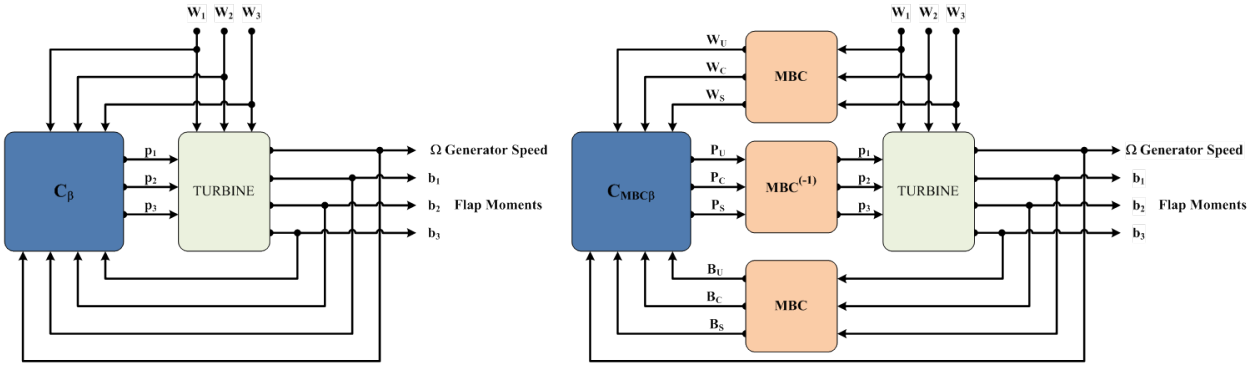


Figure 2. CART3 control approaches: (a) blade local bending-moment feedback and wind measurements; (b) MBC bending-moment feedback and wind measurements.

This report is organized as follows. The next section explains the wind conditions and turbine models in more detail. Section 3 gives an overview of the wind-speed measurement schemes considered. The subsequent two sections of the report explain the 5-MW and CART3 studies are explained in further detail. Augmentation of the baseline controllers with feedforward compensation for the 5-MW turbine model is discussed in Section 4, and the CART3 MIMO techniques and results then are presented in Section 5. The approach used in the CART3 studies is one variant of what is referred to in the literature as "preview control." Except for two appendices, the report in Section

6 concludes by discussing the results and the plans for future work. Appendix A explains the manipulation of the CART3 models for use in MIMO controller design, and Appendix B details the design of the MIMO, combined feedforward-feedback controllers.

# 2 Turbine Models and Site Conditions

All simulations are performed using the full non-linear turbine model provided by the FAST (Jonkman et al. [2]) software code developed at the National Renewable Energy Laboratory (NREL). This code reads in specified files describing wind field velocities and then applies the wind speeds to the turbine to compute the resulting turbine response. These computations involve the aeroelastic interaction between the wind and the turbine structure. The wind input can be specified in a number of different formats. This study uses the NREL TurbSim (Kelley et al. [3]) stochastic full-field inflow simulator to generate realistic wind fields for input to FAST. The following sections discuss specific turbine parameters and simulation conditions for both the 5-MW and CART3 simulations.

## 2.1 Turbine Models

The turbines modeled in FAST have the specifications shown in Table 1. The scale of the 5-MW turbine dwarfs the CART3 and, as such, has more severe pitch-rate limitations. The CART3 has an unusually high maximum pitch rate relative to most utility-scale turbines, but is typical in its power rating for its 40-meter diameter rotor.

Table 1. Turbine Specifications

| Turbine | Hub Height [m] | Rotor Diameter [m] | Max. Pitch Rate [deg/s] | Rated Gen. Torque [kN-m] | Rated Rotor Speed [rpm] | Rated Gen. Speed [rpm] | Rated Power [kW] |
|---|---|---|---|---|---|---|---|
| 5-MW | 90 | 126 | 8 | 43,094 | 12.1 | 1,173.7 | 5,000 |
| CART3 | 36.6 | 40 | 18.7 | 3,581 | 41.7 | 1,800 | 675 |

The differences in scale between the two turbines also are manifest in the characteristic frequencies associated with their structural modes, as can be observed in Table 2. FAST allows certain sections of the turbine to be modeled as rigid or flexible— each mode of flexure or displacement is referred to as a degree of freedom (DOF). For the purposes of design a restricted set of DOF are active as listed in Table 2; during simulation all available DOF provided by FAST (except for teeter) are active as listed in Table 3.

FAST is used to linearize the turbine at various operating points to obtain models used in the design of controllers. Table 2 lists the DOF enabled in obtaining design models for the various control loops. The 5-MW CP and IP feedback-only designs (CPFB; IPFB) are gain-scheduled designs and are linearized at "varied" operating points. The mode associated with the drivetrain essentially is independent of operating point and, when enabled, its characteristics do not change. The feedforward zero phase error tracking controller's (FFZPETC) feedforward compensator is designed at a single AR operating point. Similarly, the tower and blade damping feedback loops (FA-TD and FA-TBD) are designed for a single operating point, but only the blade-flap and/or tower fore-aft DOF (the modes targeted by these loops) are active during linearization. The other 5-MW feedforward controls not listed in Table 2 are based on static relationships which are independent of turbine characteristic frequencies. The CART3 controllers all are designed for a single AR operating point and take into account generator, drivetrain, and blade-flap modes in their design.

Table 2. Degrees of Freedom Enabled for Linearization and Frequency and Damping Ratio Results for Enabled Modes

| Turbine | Cont roller | Design Modes | | | | | | | |
|---|---|---|---|---|---|---|---|---|---|
| | | Generator | | Drive Train | | Blade 1st Flap | | Tower Fore-Aft | |
| | | Freq. [Hz] | Damping | Freq. [Hz] | Damping | Freq. [Hz] | Damping | Freq. [Hz] | Damping |
| 5-MW | CPitchFB | varied | varied | – | – | – | – | – | – |
| | IPitchFB | varied | varied | 2.24 | 0.052 | 0.73 | 0.58 | – | – |
| | FFZPETC | 0.040 | 1.00 | | | | | – | – |
| | FA-TD | – | – | – | – | – | – | 0.33 | 0.055 |
| | FA-TBD | – | – | – | – | 0.73 | 0.58 | | |
| CART3 | ALL | 0.031 | 1.00 | 3.5 | 0.002 | 2.1 | 0.17 | – | – |

Table 3. Degrees of Freedom Enabled for Simulation

| Simulation Modes | | | | | | |
|---|---|---|---|---|---|---|
| Generator | Drivetrain | Blade Flap 1st & 2nd | Blade Edge | Yaw | Twr F-A 1st & 2nd | Twr S-S 1 st & 2nd |

More detail on the 5-MW turbine model and the 5-MW baseline controller described in Section 4.3 can be found in the NREL report by Jonkman et al. (2009) [1].

### 2.2 Wind Conditions

The boundary conditions for the TurbSim simulator shown in Table 0.2 are derived from the averages of sub-populations of actual measured wind conditions. The (Y-Z) grid encompassing the turbine rotor disk contains 31 x 31 points of 3 orthogonal wind components with a sample rate of 20 Hz and a total record length of 630 seconds. The turbulence boundary conditions within each of the 3 wind-speed categories are varied by the vertical stability parameter ($Ri_{TL}$) and the mean friction velocity (shearing stress) ($u_{*_D}$) over the rotor disk. A power law variation of the vertical wind-speed profile is specified by the listed shear exponents ($\alpha_D$). For each row of Table 0.2, 31 realizations of the turbulent wind field based on the specified boundary conditions were generated.

## 3 Wind-Speed Measurements

The wind fields used in simulation are marched forward through the appropriate turbine without evolving over time, therefore a preview of the wind speeds that will hit the turbine can be obtained simply by taking measurements at a distance ahead of the turbine. The FAST code was edited to output these measurements for use by the designed controllers. This section explains the measurement locations used for the 5-MW and the CART3 controllers.

### 3.1 Five-Megawatt Wind-Speed Measurements

The wind measurements used in IP feedforward controllers are taken at locations that rotate with the blades so that wind speeds at the future blade positions are known in advance according to the desired amount of preview. On the other hand, the wind measurements used for CP feedforward are obtained using an average of five stationary measurement locations positioned in planes ahead of the turbine at the desired preview distances.

Figure 3(a) shows a comparison of the CP/stationary measurement with two other options for obtaining the same information. The smoothest curve is the wind-speed estimate, which requires no LIDAR, and instead is based solely on generator speed, generator torque, and blade pitch. This estimate was calculated by following a published method (Ostergaard et al. [9]); for simplicity, however, the drivetrain torsion was ignored in the calculation of aerodynamic torque. The least smooth curves are the hub-height-only wind measurements. Both a delayed preview and an "at-tower" version are plotted to show that there is very little error between the two with this simulation method. On average, the hub-height-only wind-speed measurements are a little too high as compared to the average wind speed over the rotor plane, because the wind speed varies with height according to a power law.

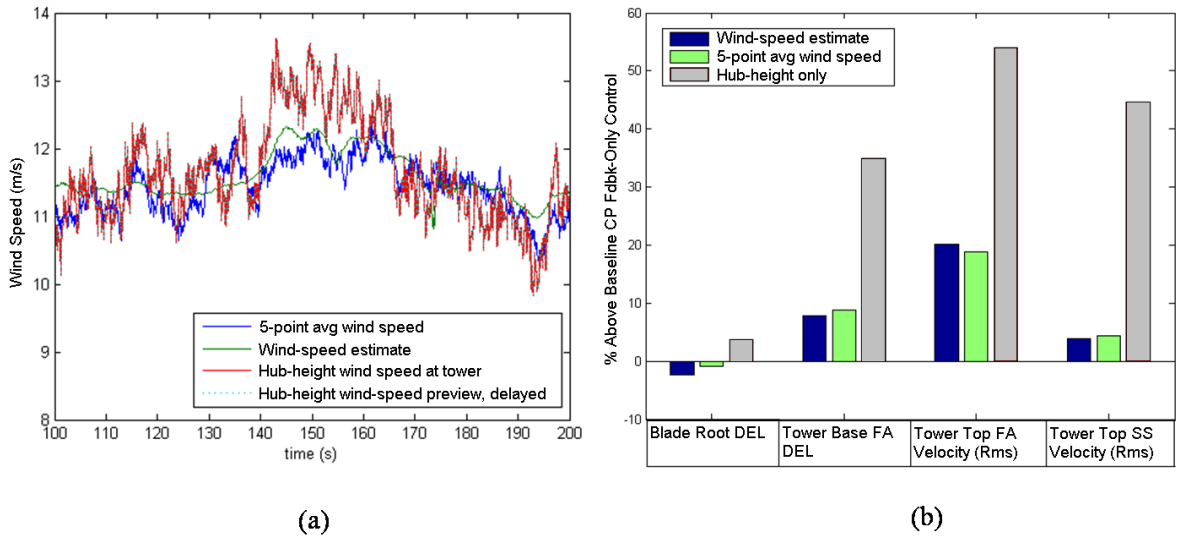


Figure 3. Considerations for 5-MW wind measurements: (a) time series comparison of different wind measurements; (b) structural loads comparison with different wind measurements— the wind measurement obtained using each of the 3 methods in the legend above is fed into the CP ZPETC feedforward with CP feedback controller showing that the 5-point average is a good choice (the wind-speed estimate cannot easily be extended to provide preview feedforward).

The three wind-measurement techniques (wind-speed estimate, 5-point average, and hub-height-only) each were tested as input to the collective-pitch ZPETC feedforward controller in a single wind field run (AR1_s1, one realization of AR1). As shown in Figure 3(b), the wind-speed estimate performed similarly to the 5-point average measurement, and the hub-height-only measurement performed significantly worse. The wind-speed estimate method is applicable only to the CP ZPETC and CP constant controllers, and not to the CP shaped controller, which requires a 5-

second preview.

## 3.2 CART3 Wind-Speed Measurements

Disturbance feedforward information for the CART3 studies is obtained using three point measurements of wind ahead of the turbine. One set of simulations uses idealized best-case measurements that rotate with the blades and another set uses stationary measurements. As explained below, the idealized measurements provide very accurate blade-local wind speeds, but speeds interpolated from stationary measurements are inherently prone to error in complex wind fields.

### *3.2.1 Basic Multi-Blade Coordinates*

In both the rotating and the stationary measurement schemes, multi-blade coordinates (MBC) are used for interpolation. In the rotating scheme, MBC is used to predict blade locations at the preview time based on their present position and rotor speed. In contrast, the stationary wind-speed measurements are interpolated to estimate the wind speeds at the location the blades will arrive at after the preview time has elapsed. An explanation of this interpolation from stationary measurements provides a relatively straightforward introduction to MBC. We start by assuming that the wind variation across the rotor plane is perturbed away from nominal by a uniform change across the rotor disk, and also by linear horizontal and vertical shear.

Shear typically is quantified in terms of the change in wind speed seen at the blade tips as a (unitless) fraction of the spatial average wind speed ($\mathrm{w}_0$) across the rotor disk. Perturbations are defined in a manner consistent with FAST. If the horizontal wind speed is perturbed away from the nominal ($\mathrm{w}_0$) due to a uniform (spatially within the rotor plane) amount ($\mathrm{w}_u$), as well as by horizontal ($\Delta_h$) and vertical ($\Delta_v$) shear components, then the total perturbation ($\Delta_x$) at a location with horizontal and vertical coordinates $(y, z)$ within the rotor disk is as follows

$$\Delta_x(y,z) = \Delta_v \frac{\mathrm{w}_0}{2}\frac{z}{R} + \Delta_h \frac{\mathrm{w}_0}{2}\frac{y}{R} + \mathrm{w}_u, \tag{1}$$

where $R$ is the radius of the rotor disk. The factor of one half appears because FAST applies only half the shear perturbation on each side of the rotor disk.

To express the perturbation in MBC, the $z$ and $y$ coordinates simply are expressed as a function of rotor azimuth. Facing the turbine from a position upwind, let $\theta$ represent the clockwise azimuth of blade 1 (the convention used by FAST) from upward vertical, and let $r_0$ represent the radius at which the wind speed is measured. The measurement position at radius $r_0$ along blade 1 is $(y, z) = (-r_0 sin(\theta), r_0 \cos(\theta))$ so that the perturbation is computed as a function of azimuth as shown below.

$$\begin{aligned}\Delta_x(\theta) &= \Delta_v \frac{\mathrm{w}_0}{2}\frac{r_0}{R}\cos(\theta) - \Delta_h \frac{\mathrm{w}_0}{2}\frac{r_0}{R}\sin(\theta) + \mathrm{w}_u \\ &= \mathrm{w}_c \cos(\theta) + \mathrm{w}_s \sin(\theta) + \mathrm{w}_u\end{aligned} \tag{2}$$

So, the MBC perturbations $[\mathrm{w}_u, \mathrm{w}_c, \mathrm{w}_s]$ observed at rotor azimuth $\theta$ and radius $r_0$ are related to shear perturbations $[\Delta_v, \Delta_h]$ by the following.

$$\mathrm{w}_{mbc} = \begin{bmatrix}\mathrm{w}_u \\ \mathrm{w}_c \\ \mathrm{w}_s\end{bmatrix} = \begin{bmatrix}1 & 0 & 0 \\ 0 & \frac{\mathrm{w}_0}{2}\frac{r_0}{R} & 0 \\ 0 & 0 & -\frac{\mathrm{w}_0}{2}\frac{r_0}{R}\end{bmatrix} \begin{bmatrix}\mathrm{w}_u \\ \Delta_v \\ \Delta_h\end{bmatrix} = M_{m2s}^{-1}\ \mathrm{w}_{sh} \tag{3}$$

The matrix $(M_{m2s})$ scales from MBC perturbations to equivalent shear perturbations. Repeating equation (2) at each blade azimuth gives the basic MBC transformation that computes the MBC components as a function of rotor position from individual, blade-local measurements $[\mathrm{w}_1, \mathrm{w}_2, \mathrm{w}_3] = [\Delta_x(\theta), \Delta_x(\theta + \frac{2\pi}{3}), \Delta_x(\theta + \frac{4\pi}{3})]$ made along each blade at radius $(r_0)$ as shown below.

$$\mathrm{w}_{mbc} = \begin{bmatrix}\frac{1}{3} & \frac{1}{3} & \frac{1}{3} \\ \frac{2}{3}\cos(\theta) & \frac{2}{3}\cos(\theta + \frac{2\pi}{3}) & \frac{2}{3}\cos(\theta + \frac{4\pi}{3}) \\ \frac{2}{3}\sin(\theta) & \frac{2}{3}\sin(\theta + \frac{2\pi}{3}) & \frac{2}{3}\sin(\theta + \frac{4\pi}{3})\end{bmatrix} \begin{bmatrix}\mathrm{w}_1 \\ \mathrm{w}_2 \\ \mathrm{w}_3\end{bmatrix} = T(\theta)^{-1}\ \mathrm{w} \tag{4}$$

The convention for denoting the MBC transform by the inverse of $T(\theta)$ is convenient for computing the MBC transformation of the linearized turbine model, as outlined in Appendix A2. The relationship in equation (4) is exact if the perturbation is due only to uniform and linear shear. Otherwise, this relationship can be viewed as a means of estimating average shear (via $M_{m2s}$) from individual point measurements. Similarly, if the MBC perturbation ($\mathrm{w}_{mbc}$) is known then the blade-local wind perturbations measured at the blades when the rotor azimuth angle is $\theta$ are given by the inverse MBC transformation.

$$\mathrm{w} = \begin{bmatrix}1 & \cos(\theta) & \sin(\theta) \\ 1 & \cos(\theta + \frac{2\pi}{3}) & \sin(\theta + \frac{2\pi}{3}) \\ 1 & \cos(\theta + \frac{4\pi}{3}) & \sin(\theta + \frac{4\pi}{3})\end{bmatrix} \mathrm{w}_{mbc} = T(\theta)\ \mathrm{w}_{mbc} \tag{5}$$

Again, if the shear data is for average variation across the rotor disk, then the relationship above is exact if the total wind variation is due only uniform and linear shear components. Otherwise, it is an estimate of blade-local speeds from average data. As used in this study, the MBC (or, equivalently, shear) components originate as estimates computed from single point measurements.

### 3.2.2 Stationary and Rotating Wind Measurements

A version of the FAST code is modified to output three wind measurements.

$$\begin{bmatrix}\mathrm{w}_1 \\ \mathrm{w}_2 \\ \mathrm{w}_3\end{bmatrix} = \begin{bmatrix}\Delta_x(x_1 - x_{prev},\ y_1,\ z_1) \\ \Delta_x(x_2 - x_{prev},\ y_2,\ z_2) \\ \Delta_x(x_3 - x_{prev},\ y_3,\ z_3)\end{bmatrix} \tag{6}$$

These are taken at a distance of $x_{prev} = \tau_{prev} * \mathrm{w}_0$ ahead of the turbine corresponding to $\tau_{prev} = 0.45$ seconds at the average wind speed $\mathrm{w}_0$ for the simulation. The measurements are equally spaced around $2\pi$ radians at a radius equivalent to 75% span of the blades. The FAST code is written to advance the TurbSim wind file past the turbine at the average wind speed $\mathrm{w}_0$ and this is known a priori, therefore the exact distance $x_{prev}$ corresponding to the desired preview time is known. In this way, it is possible to get very accurate measurements of the wind-speed variations that will arrive at each blade.

In the stationary measurement mode, the measurements always are taken with $\mathrm{w}_1$ at vertical ($\theta = 0$) and the other two locations spaced at multiples of $2\pi/3$ radians. The MBC components then are computed according to equation (4) with $\theta = 0$. The rotor position expected after the preview time has elapsed is predicted according to

$$\theta_{prev} = \theta_{rotor} + \Omega \cdot \tau_{prev}, \tag{7}$$

where $\Omega$ is the present rotor speed. The wind speeds that the blades will experience at the preview position are estimated from the stationary measurements by interpolating to the predicted blade locations using equation (5) with $\theta = \theta_{prev}$.

In the more accurate rotating mode, the present blade locations are transformed to their present MBC coordinates.

$$x_{mbc}(t) = T^{-1}(\theta) \begin{bmatrix} x_1(t) \\ x_2(t) \\ x_3(t) \end{bmatrix} \tag{8}$$

The positions then are interpolated ahead to positions at the azimuth ($\theta_{prev}$) that is expected after the elapsed preview time.

$$\begin{aligned} x(t + \tau_{prev}) =& T(\theta_{prev}) x_{mbc}(t) \\ y(t + \tau_{prev}) =& T(\theta_{prev}) y_{mbc}(t) \\ z(t + \tau_{prev}) =& T(\theta_{prev}) z_{mbc}(t) \end{aligned} \tag{9}$$

The modified FAST code simply outputs the wind speeds in front of the turbine from the expected blade positions.

$$\begin{bmatrix} \mathrm{w}_1 \\ \mathrm{w}_2 \\ \mathrm{w}_3 \end{bmatrix} = \begin{bmatrix} \Delta_x(\ x_1(t + \tau_{prev}) - x_{prev},\ y_1(t + \tau_{prev}),\ z_1(t + \tau_{prev})\ ) \\ \Delta_x(\ x_2(t + \tau_{prev}) - x_{prev},\ y_2(t + \tau_{prev}),\ z_2(t + \tau_{prev})\ ) \\ \Delta_x(\ x_3(t + \tau_{prev}) - x_{prev},\ y_3(t + \tau_{prev}),\ z_3(t + \tau_{prev})\ ) \end{bmatrix} \tag{10}$$

In effect, these measurement locations in front of the turbine rotate in coordination with predicted

blade positions. The only error in the resulting preview wind speeds is due to the error in interpolating the blade locations, and this occurs because the rotor speed isn't necessarily constant.

### 3.2.3 Comparison of Stationary and Rotating Wind Measurements

The result of stationary and rotating measurement modes for a given simulation run are displayed in Figure 4(a) where the actual wind speeds seen at 75% span are time-shifted to align with the preview measurements. The rotating measurements are shown in the top plot and are indistinguishable from the wind speeds actually encountered. The stationary preview measurements (center plot and the amplitude spectrum in the bottom plot) tend to have a low-pass filtering effect due to the MBC interpolation, and produce a visible error. Most of the error found in the stationary approach is because the wind conditions produce more than just shear variation across the rotor disk; the shear measured at the stationary locations can be significantly different than that at the actual rotor positions.

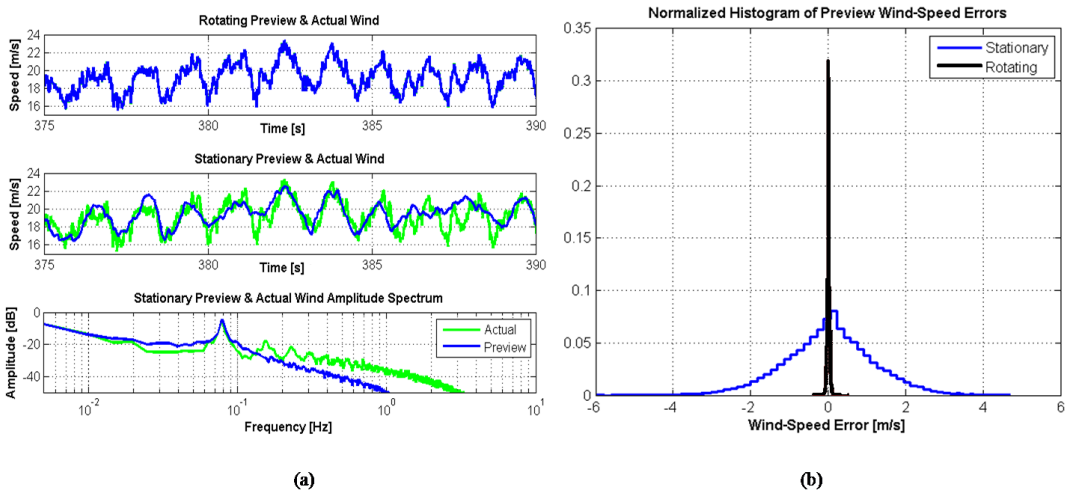


Figure 4. Wind speeds at 75% span of one blade; (a) top plot— actual wind speeds and rotating measurements (indistinguishable from each other); center plot— actual wind and speeds interpolated from stationary measurements; bottom plot— amplitude spectrum of the wind seen at the blade and that of the interpolated measurements; (b) histograms of errors relative to actual wind speeds.

The histograms shown in Figure 4(b) show the prediction errors from data taken at the 75% span of one blade during 600 seconds of simulation time. The maximum error ($\sim$ 6 m/s) produced by the stationary-interpolation scheme is greater than ten times larger than that produced by the rotating measurements ($<$ 0.5 m/s) as can be observed in Figure 4(b). Without utilizing some form of azimuth prediction (e.g. Kalman filtering or other model-based prediction), the rotating measurements are the best we currently can produce. In fact, because in reality, the wind speeds ahead of the turbine continue to evolve en route and the time to arrival is not constant (as is implemented in FAST) the rotating measurements can be considered unrealistically accurate. In future work, we also will consider the distortions and noise that are typical in LIDAR measurements.

In this study, however, the goal for the rotating scheme is to better understand the best possible outcome using preview control, and the stationary measurements serve as a first investigation into the effect of errors in wind-speed measurements.

# 4 5-MW Feasibility: Adding Feedforward to Standard Feedback Controllers in Above Rated (AR) and Near Rated (R) Conditions

## 4.1 Yaw Control

The yaw control is set to a constant 0°, and the average wind direction does not change.

## 4.2 Torque Control

The low-pass filtered generator speed also is the input to the torque controller. Torque control typically is divided into different regions depending on generator speed, as shown in Figure 5. Regions 1 and 1.5 are turbine start-up and transition regions. In Region 2, the torque command is proportional to the square of the generator speed. This maintains a constant tip-speed ratio for maximum power capture. Region 2.5 provides a transition to Region 3. Region 3 begins at rated generator speed; in this region, the torque controller maintains constant rated power and the torque command is inversely proportional to generator speed. Also in Region 3, the pitch controller actively regulates generator speed. When the wind speed drops so that the generator speed falls below Region 3, then the pitch command settles to its lower limit of 0°.

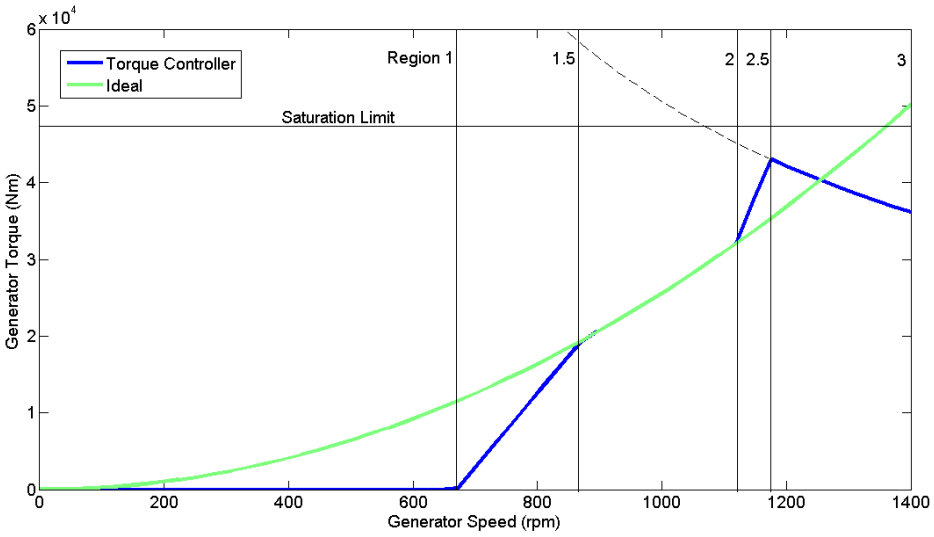


Figure 5. Baseline torque control

The torque controller has an additional feature that reduces downward spikes in power from the rated 5 megawatts. Whenever the blade-pitch angle is greater than or equal to 1°, the torque controller follows the Region 3 curve, even if the generator speed is below rated. This is represented by the dashed line in Figure 5. The torque command is limited to between 0 Nm and 47,402.91 Nm, and is rate limited to 15,000 Nm/s.

## 4.3 Baseline collective-pitch Control

The collective-pitch blade-pitch controller depends only on generator speed. The generator speed signal is fed through a low-pass filter and then into a gain-scheduled proportional-integral (PI) controller, as shown in Figure 6. Blade pitch is limited between 0° and 90° and rate limited to $8°/s$.

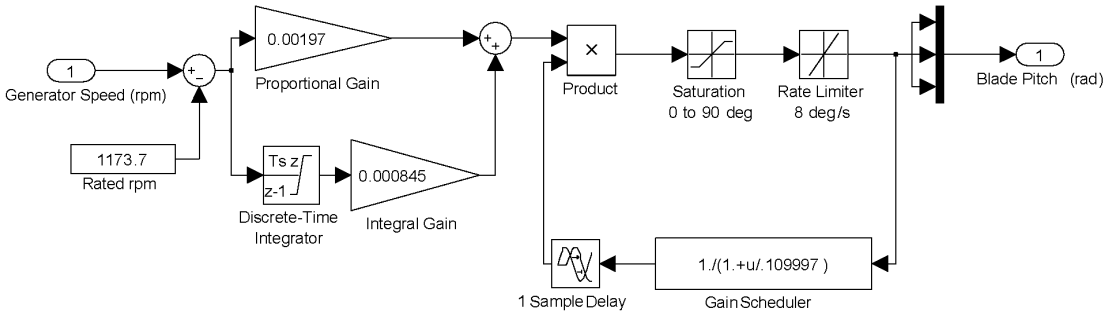


Figure 6. Simulink [15] diagram of baseline collective-pitch control

## 4.4 Baseline individual-pitch Control

An individual-pitch feedback-only controller also was designed (Bossanyi [6]) for use as another baseline controller for comparison with the individual-pitch feedforward controllers. In addition to generator speed, its inputs are the three out-of-plane blade-root bending moments and the rotor azimuth, which is used for the MBC (or d-q axis) transformation. The horizontal and vertical components are controlled with PI controllers, and the collective component is controlled with the same PI feedback control as the baseline collective-pitch controller.

## 4.5 Feedforward Control Designs

This section presents some initial ideas for feedforward control designs; these fall into one of two categories. The first is model-inverse control, designed to cancel the effect of wind disturbances on rotor speed. The second is a shaped compensator method, which is an intuitive, essentially non-model-based approach.

### *4.5.1 Gain-Scheduled Model-Inverse Feedforward Control*

The first step in designing a model-inverse feedforward controller is obtaining a linear model of the turbine ($P$). In this study the turbine is linearized about an 18 m/s constant wind speed, with five degrees of freedom turned on.

- First flapwise blade mode ($\times$ 3 blades)
- Drivetrain rotational-flexibility

- Generator

This results in two transfer functions: $P_{\Omega\beta}$, which maps collective blade-pitch error ($\beta$) to generator-speed error ($\Omega$), and $P_{\Omega w}$, which maps deviation ($w$) from nominal wind speed to generator-speed error ($\Omega$).

$$P_{\Omega\beta} = \frac{0.091923(z+1.584)(z-1.094)(z-0.922)(z-0.1628)}{(z-0.9968)(z^2-1.932z+0.9356)(z^2-1.951z+0.9819)} \tag{11}$$

$$P_{\Omega w} = \frac{0.0002991(z+1.829)(z-0.1577)(z^2-1.572z+0.6193)}{(z-0.9968)(z^2-1.932z+0.9356)(z^2-1.951z+0.9819)} \tag{12}$$

Sampling time: 0.0125 s

A feedforward controller is shown as $F$ in Figure 7. A linear model-inverse feedforward approach uses $F$ to cancel the effect of $w$ on $\Omega$. Therefore, as can be seen in Figure 7, $F$ is as follows.

$$P_{\Omega\beta} \cdot F \cdot w = -P_{\Omega w} \cdot w \tag{13}$$

$$F = -P_{\Omega\beta}^{-1} P_{\Omega w} \tag{14}$$

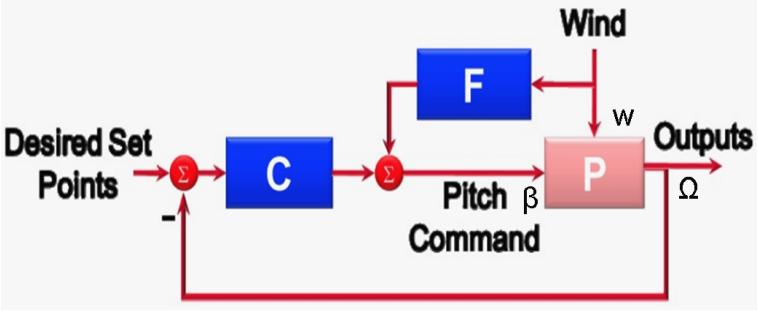


$(\Omega_{desired} = 0)$

Figure 7. Combined feedback/feedforward control with only generator speed error feedback

Ideally, the feedforward controller would be set equal to $F$ as shown above. In this case, however, the resulting $F$ is unstable because $P_{\Omega\beta}$ contains non-minimum-phase zeros. Therefore a stable model-inverse approximation is used instead. Three different model-inverse techniques (Butterworth et al. [16]) are used: the nonminimum-phase zeros ignore (NPZ-Ignore), the zero-phase-error tracking controller (ZPETC), and the zero-magnitude-error tracking controller (ZMETC).

$$F_{NPZ\text{-}Ignore} = \frac{0.013418(z+1.829)(z-0.1573)(z^2-1.572z+0.6194)}{z^2(z-0.922)(z-0.1628)} \tag{15}$$

$$F_{ZPETC} = \frac{0.09587(z+1.829)(z+0.6313)(z-0.9142)(z-0.1573)(z^2-1.572z+0.6194)}{z^4(z-0.922)(z-0.1628)} \tag{16}$$

$$F_{ZMETC} = \frac{0.001878(z+1.829)(z-0.1577)(z^2-1.572z+0.6193)}{(z-0.1628)(z-0.9142)(z-0.922)(z+0.6313)} \tag{17}$$

Sampling time: 0.0125 s

When simulated in a uniform wind field, stepped from 15 m/s to 20 m/s, all three controllers perform similarly and show some improvement over baseline (as shown in Figure 8), even without any gain scheduling or low-pass filtering. The feedforward controller increases blade-pitching action to keep rotor speed more constant and to reduce the magnitude of oscillations in blade-root bending moment. The controllers shown here use wind-speed measurements at the blades with no preview.

All controllers studied are discrete-time controllers with a sample period of 0.0125 s. The ZPETC requires an added delay of $z^{-2}$ (two sample periods, or 0.025s) to make the controller causal. A 0.025 s preview cancels this delay, making the phase of this controller match the ideal case exactly. The NPZ-Ignore and ZMETC require no added delay, so an instantaneous wind-speed measurement at the blades is ideal for these controllers.

One wind-speed measurement that has been made available in the simulation is an approximate disc-average of the u-direction (towards turbine) wind speed, measured 90 m ahead of the turbine tower. Measurements at five points of the 90 m-ahead disc are used to obtain this approximate average: hub center, and 63 meters straight up, down, left, and right. The wind fields used in simulation can be thought of as a three-dimensional grid, with three wind-speed directional components at each point in the grid. It does not evolve over time, but is marched forward towards the turbine at a constant rate, equal to the average wind speed of the particular wind field being used. Therefore, the 90 m-ahead wind-speed signal can be delayed without any loss of accuracy. For inputs to the ZPETC, NPZ-Ignore, and ZMETC controllers, the signal is delayed so that it is approximately at the blades, which are about 6 m ahead of the tower. Because the blades do not lie in a perfect plane—they are preconed forward by 2.5° and bend back somewhat during operation—it is not possible to choose the distance precisely or to choose the delay accurately to within 0.025 s.

All three controllers have a fixed DC gain of approximately 0.0234 rad/(m/s). These controllers perform best when operating close to the linearization point of 18 m/s wind speed. To improve performance over a greater range of wind speeds, the DC gain of the feedforward controllers is adjusted based on wind speed. The ideal gain values are based on testing of the non-linear turbine model at various points over a range of wind speeds from 11.4 m/s to 25 m/s to find the required steady-state blade pitch at each point such that $\Omega = 0$.

The wind-speed input to this gain scheduler first is fed through an eighth-order low-pass Butterworth filter that filters out anything greater than or equal to the once-per-revolution frequency of 0.2 Hz. This stops high frequencies from being passed through to the blade-pitch signal.

Early testing of the collective-pitch gain-scheduled model-inverse feedforward controllers showed that results improved when a low-pass filter also is applied to the input signal to the controller itself. This filter is a single-pole low-pass filter with a corner frequency of 0.025 Hz. This removes much of the dynamics of the controller, however, leaving it essentially equivalent to a low-pass filter multiplied by a (gain-scheduled) constant. It therefore appears that these controllers are not working as expected, except at low frequencies. This could be because the required amount of delay cannot be made precise enough, or because the higher frequencies in the five-point average are not representative of the entire disc. Some of the problem also might be due to operation far from the linearized operating point, and it is possible that this could be corrected by scheduling not only the gain at different wind speeds, but also the locations of controller poles and zeros. It is interesting to note, however, that when the turbine model is linearized using only two degrees of freedom

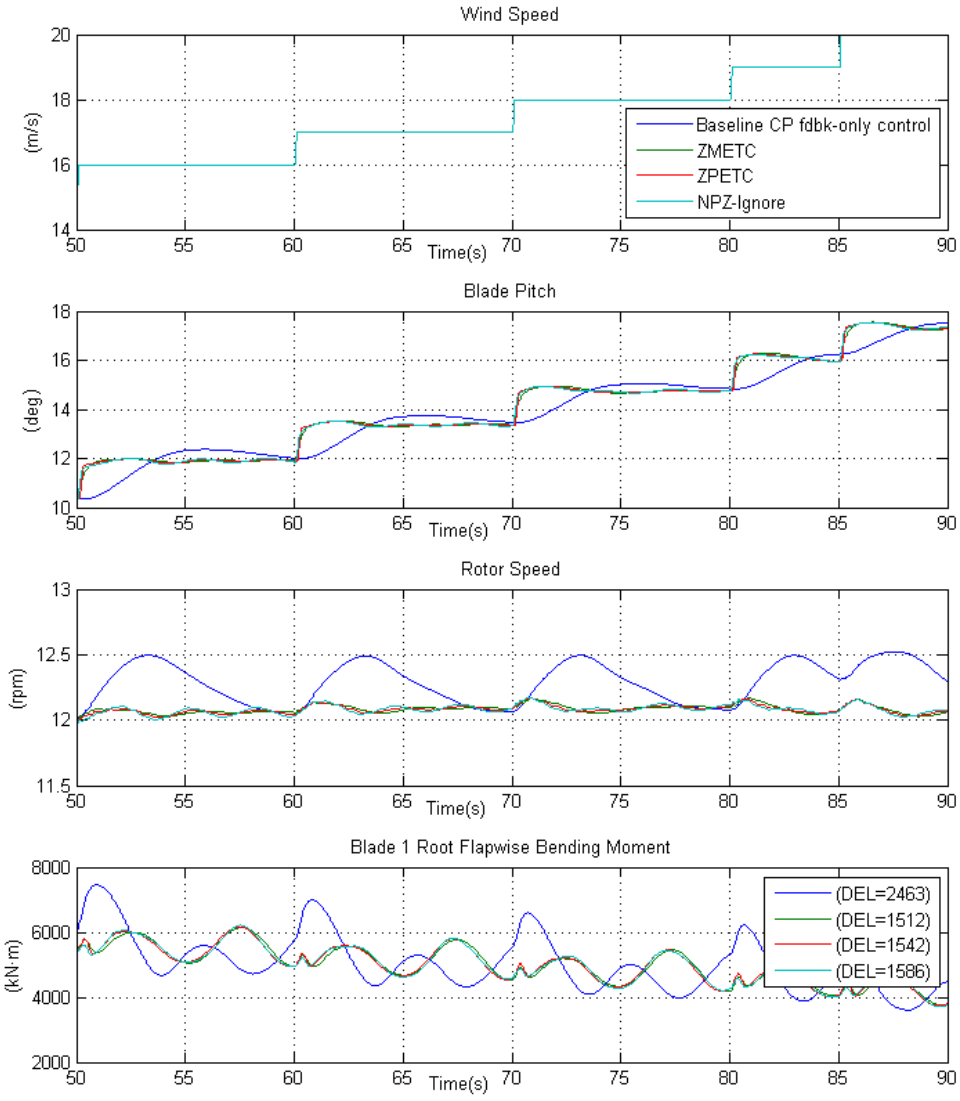


Figure 8. Comparison of model-inverse and baseline control with simulations in uniform stepped wind; root-bending moments are compared using damage equivalent loads (DEL)

(drivetrain rotational-flexibility and generator) instead of five, $P_{\Omega w}$ and $P_{\Omega \beta}$ have almost identical dynamics, so the ideal model-inverse controller, $F = -P_{\Omega \beta}^{-1} P_{\Omega w}$, simply is equal to a constant of approximately 0.0234 rad/(m/s).

Testing of the three controllers shows that all produce similar results. The simulation results for the ZPETC with low-pass filter on both the gain scheduler and the input therefore are used as representative of all three. For comparison, simulation results for a low-pass-filtered gain-scheduled constant also are presented.

These two controllers originally were collective pitch. Individual-pitch versions also were designed. Each individual-pitch version has three wind-speed inputs, one at each blade at approximately 75% span. It simply uses the same collective-pitch controller three times, once for each blade. The low-pass filter pole at 0.025 Hz is increased to allow the 0.2 Hz ($1P$) signal through so that the individual-pitch controller can handle wind shear.

### 4.5.2 Gain-Scheduled Shaped Compensator Feedforward Control

Rather than using an instantaneous wind-speed measurement at the blades, or a few hundredths of a second ahead of the blades, the shaped compensator uses an advance wind measurement up to five seconds ahead of the blades. This gives the blades more time to react to changes in wind speed and keeps pitch rates to more reasonable levels.

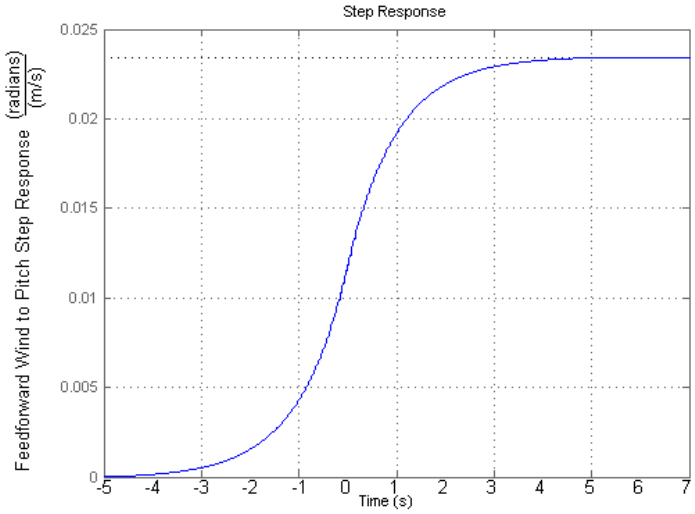


Figure 9. Desired step response of feedforward shaped compensator (rad/(m/s))

First, the desired step response shown in Figure 9 is created. The step change in wind speed hits the blades at the 0 s mark on the plot, where the blade pitch is rising the fastest. The step response completely determines a linear controller. To find the transfer function for this controller, take the derivative of the step response to obtain the continuous-time impulse response, as shown in Figure 10.

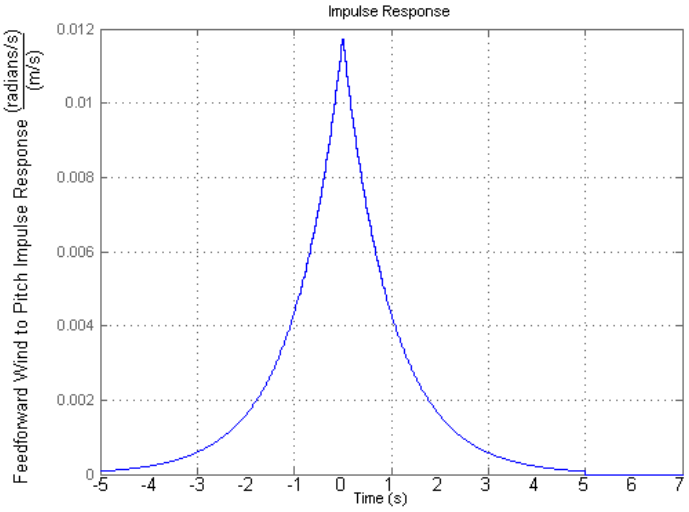


Figure 10. Desired continuous-time impulse response of feedforward shaped compensator ((rad/s)/(m/s))

To determine a discrete-time controller with sample period 0.0125 s, the continuous-time impulse response is sampled every 0.0125 s and multiplied by 0.0125 to yield the discrete-time controller pulse response. The transfer function then simply is $b_{-n}z^n \ldots + b_{-2}z^2 + b_{-1}z^1 + b_0 + b_1z^{-1} + b_2z^{-2} \ldots + b_nz^{-n}$, where $b_i$ is the value of the pulse response at sample $i$ (at time $0.0125i$), and here $n = 400$, because the pulse response starts 400 samples (5 s) before time 0. This feedforward controller transfer function can equivalently be written as follows.

$$F(z) = \frac{b_{-n}z^{2n} \ldots + b_{-2}z^{n+2} + b_{-1}z^{n+1} + b_0z^n + b_1z^{n-1} + b_2z^{n-2} \ldots + b_n}{z^n}$$

This is an 800th-order non-causal FIR (finite impulse response) compensator.

To actually implement this non-causal compensator, first its transfer function is multiplied by $z^{-n}$, making it causal. The wind-speed input to this causal compensator is 5 s ahead of the blades, rather than directly at the blades. This is effectively a multiplication of the wind-speed input by $z^n$, which cancels the $z^{-n}$. This compensator then is gain scheduled exactly as described for the model-inverse feedforward controller. In this case, the low-pass filter is applied to the gain scheduler but not to the feedforward compensator input. This controller also originally was collective pitch. An individual-pitch version is designed by using three copies of the collective-pitch controller, one for each blade. There then are three separate wind-speed measurement inputs, 5 s ahead of each blade at 75% span.

The shaped compensator idea also can be evaluated at different wind-preview lengths. In addition to the 5 s preview version, we consider 10/3 s preview and 5/3 s preview versions of the individual-pitch shaped compensator. These were designed by shrinking the step response to 2/3 and 1/3 of its original length.

### 4.5.3 Phasing Out individual-pitch Controllers

As the wind speed drops below rated, the individual-pitch controllers are phased out of operation using the phase-out block shown in Figure 11. The lower blade-pitch limit for this turbine model is 0°. Without a phase-out block, as the wind speed drops below rated the controller causes the pitch of each blade to saturate at 0°. This causes a problem for independent pitch control because each pitch command is approximately sinusoidal at the rotational frequency of the turbine, and when the part of the sinusoid below 0° is cut off, the average pitch command becomes greater than desired, causing reduced rotor speeds and reduced power capture. At near-rated wind speeds, where part of the sinusoids are below 0°, the phase-out block works to keep the average pitch at the correct value, and reduces the amplitude of each sinusoid until it just reaches but does not go below 0°. This is done in the individual-pitch feedforward controllers as follows.

The phase-out block has a three-element vector input $\beta_{in}$ and three-element vector output $\beta_{out}$, with one element for each blade pitch command. First, an instantaneous average of the three pitch commands is taken.

$$\text{avg} = \frac{\beta_{in}(1) + \beta_{in}(2) + \beta_{in}(3)}{3}$$

The difference between that average and the pitch command farthest from that average at any given time is then taken.

$$d = \max(|\beta_{in}(1) - \text{avg}|, |\beta_{in}(2) - \text{avg}|, |\beta_{in}(3) - \text{avg}|)$$

Now $d$ provides an approximate value of the amplitude of the three $\beta_{in}$ sinusoids but, as a function of time, it contains an undesirable ripple. Therefore it is fed into a low-pass filter and the output of the low-pass filter is increased by about 5% to match the peak rather than the center of the ripple. This gives an estimate of the current amplitude ($amp$) of the three commanded signals $\beta_{in}$. The commanded signals then are passed through with the same average value, but with the amplitude scaled down so that it just reaches the 0° limit.

$$\beta_{out} = \text{avg} + (\beta_{in} - \text{avg}) * (\text{avg}/amp)$$

Inputs and outputs to this process are shown in Figure 12.

A different method was used in the baseline individual-pitch controller, taking advantage of the MBC transformation. In this case, the current amplitude is found as follows.

$$amp = \sqrt{\beta_v^2 + \beta_h^2}$$

Where $\beta_v$ and $\beta_h$ are the vertical and horizontal components of commanded pitch signals. As done in the feedforward controller phase-out scheme described above, this amplitude then is scaled down so that it just reaches the 0° limit. Because the baseline individual-pitch controller is feedback and not feedforward, an additional complication also appears. Anti-windup must be added so that integrator windup does not occur in cases where the amplitude of the individual-pitch commands does need to be scaled down.

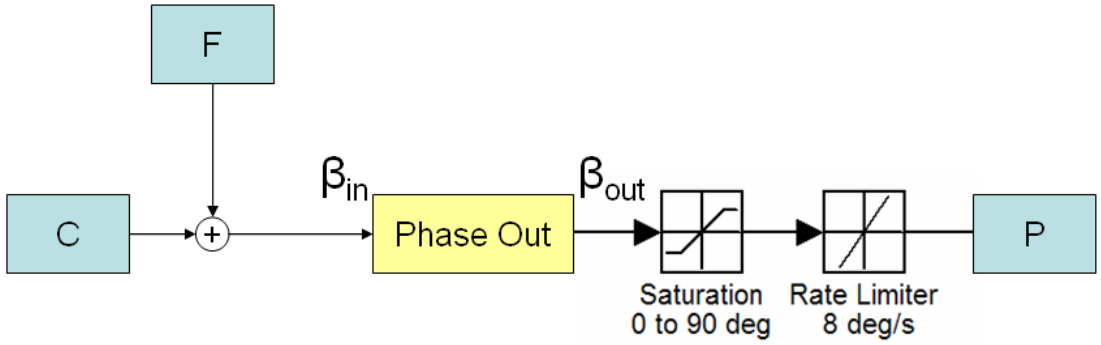


Figure 11. Phase-out block for individual-pitch control shown with 3-element vector input $\beta_{in}$ and output $\beta_{out}$ (F: feedforward control, C: feedback control, P: plant (wind turbine))

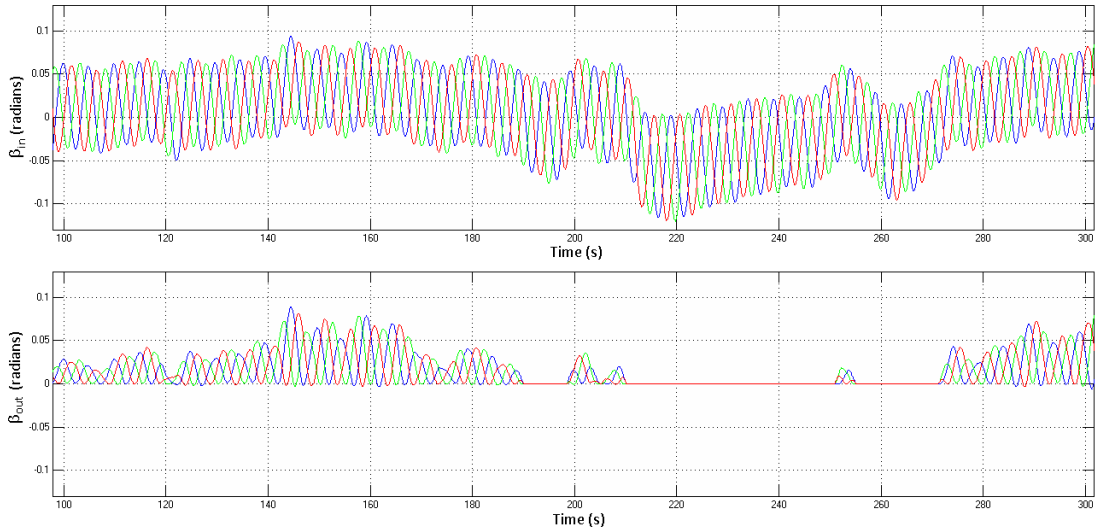


Figure 12. Sample input and output to individual-pitch control phase-out block

## 4.6 Simulation Results

All controllers were simulated in the above-rated and rated wind fields listed in Table 0.2 for the 5-MW turbine. A comparison of structural loading measures, averaged over all wind fields, is provided in Figure 13. These measures include rms nacelle velocities and damage equivalent loads of blade and tower bending moments. Damage equivalent loads are calculated using code from NREL based on a rainflow-counting algorithm (Downing et al. [17]), also used in the NREL code CRUNCH and the Sandia code LIFE2, with a Wohler curve exponent of 10, typical for composite material. Note that the side-to-side tower-top rms velocity measure had initial transients that took much longer to settle than the others, sometimes more than 100 s. Only the first 99 s of each run were discarded to allow for settling, therefore this particular measure might not have actually increased as much as these plots show.

On the left side of Figure 13, the three collective-pitch feedforward controllers are compared to the collective-pitch feedback-only baseline control. Although these controllers show a small reduction in blade-root loads at above-rated wind speeds, their overall performance is worse than that of the baseline controller. The two plots on the left also show that the baseline individual-pitch controller overall is an improvement over the baseline collective-pitch controller, at least at above-rated wind speeds.

On the right side of Figure 13, the six individual-pitch feedforward controllers are compared to the individual-pitch feedback-only baseline control. Three of these are an improvement over baseline: IP Shaped 5 s Feedforward with CP Feedback, IP Shaped 10/3 s Feedforward with CP Feedback, and IP Shaped 5 s Feedforward with IP Feedback. These three designs each incorporate a preview measurement of the incoming wind speed at three points ahead of the turbine. These three designs also do not reduce power production, and even allow tighter regulation of power production and rotor speed, as can be seen in Figure 14 and Figure 15. Figures 14 and 15 also show that the feedforward controllers increase pitch rates but still operate within a limit of $8°/s$. Comparing the above-rated (AR) results to the near-rated (R) results, we see that more reduction of structural loads is possible in the AR case than in the R case, where pitch control often is limited by the 0° minimum. The next section covers the CART3 controllers and results. A discussion of both sets of results can be found in Section 6.

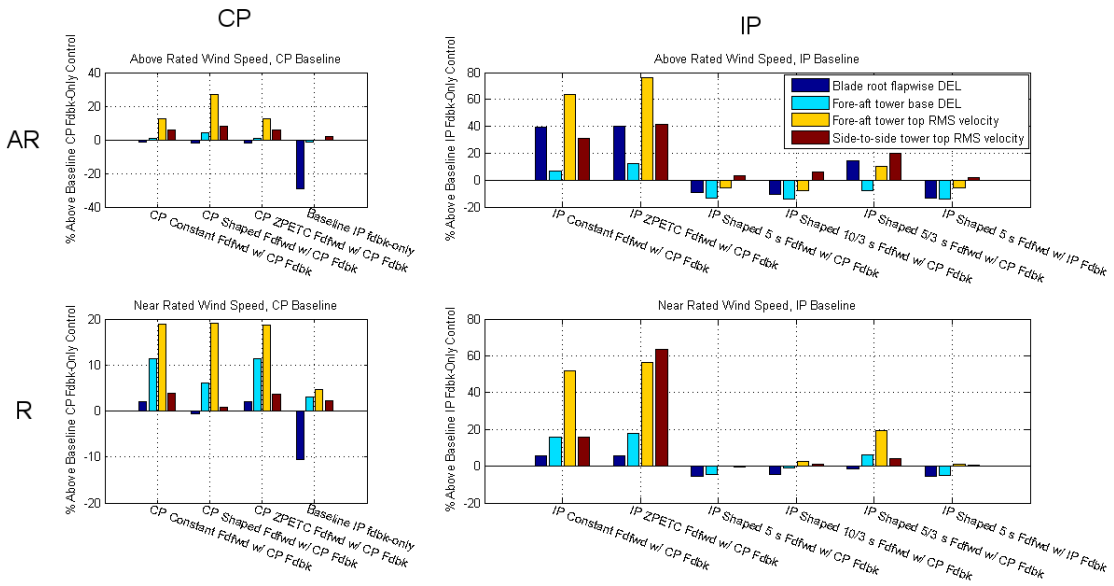


Figure 13. Structural loads comparison; the two left plots show that IP feedback is a big improvement over CP feedback, greatly reducing blade-root loads; the two right plots show additional load reduction when 5 s or 10/3 s of preview feedforward is added to IP feedback or to CP feedback; the best controller is on the far right

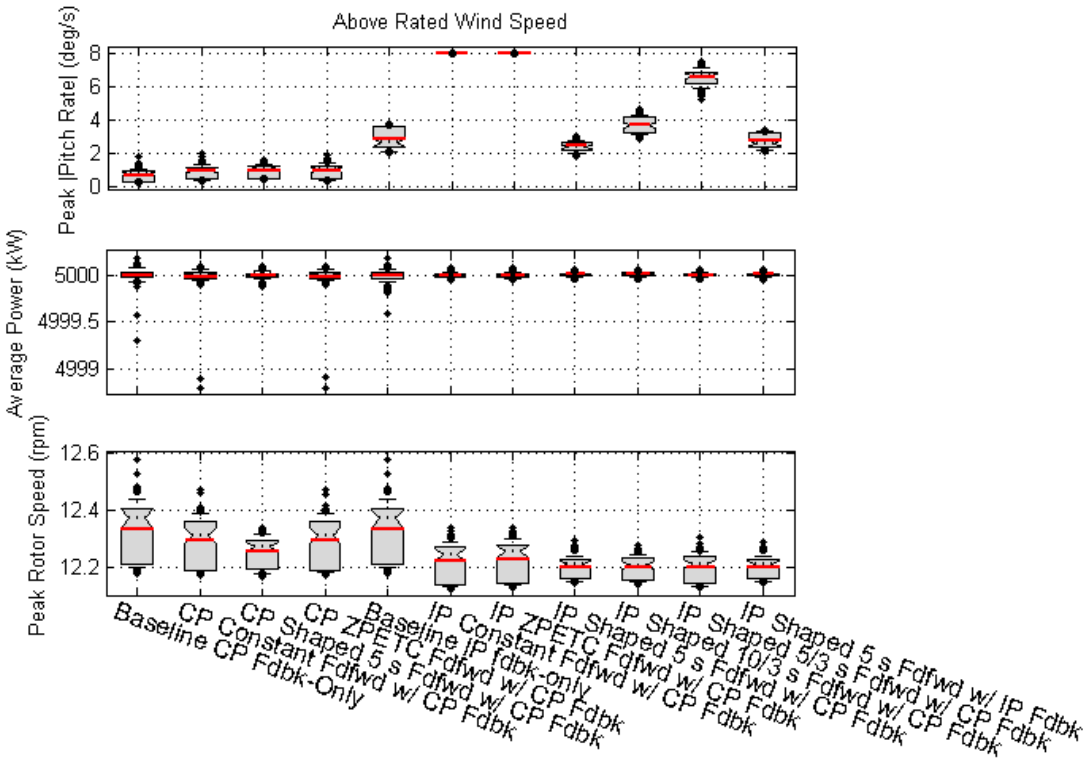


Figure 14. Peak pitch rate, average power production, and peak rotor speed for above-rated wind fields; the box plots have lines at the lower quartile, median, and upper quartile values; a solid red line shows the mean (the median is a plotted with a black dotted line); the whiskers extend to the 10th and 90th percentiles; large black dots indicate the extent of the 5th and 95th percentiles; outliers are data with values beyond the dots; each dot is one of the 93 AR runs; the larger the number of sample runs, the narrower the notches in the sides of the boxes become; if one box's notches do not vertically overlap with another box's, this indicates with 95% confidence that the true medians of those two boxes do differ

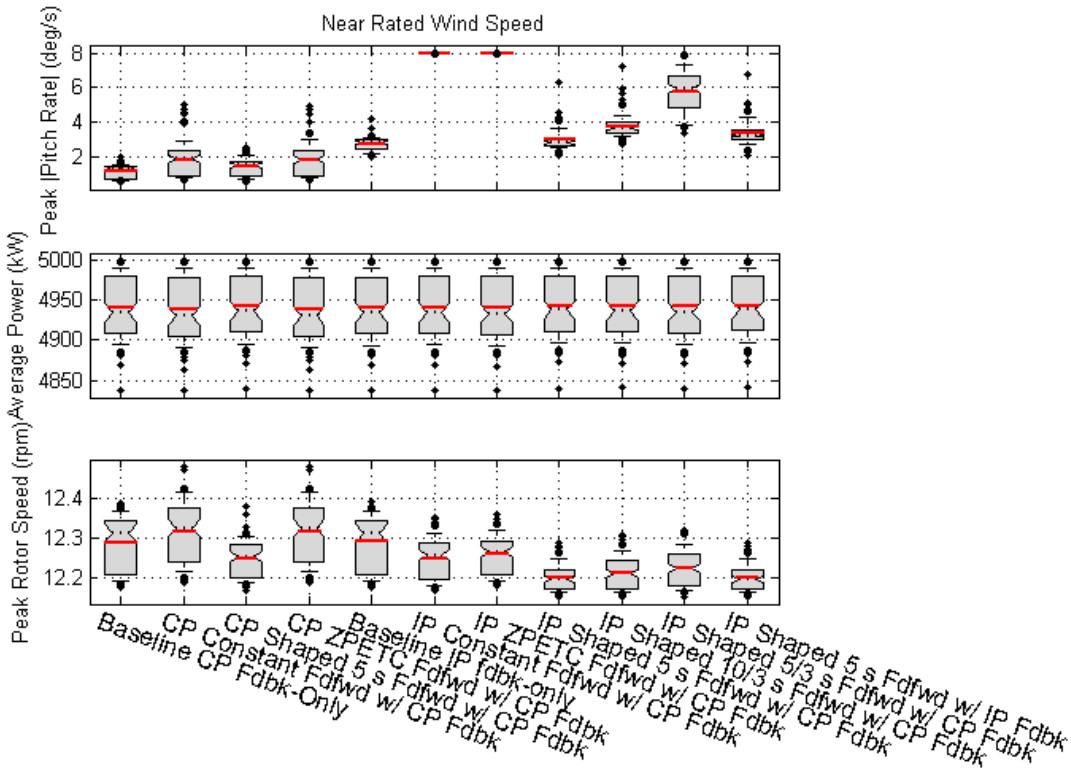


Figure 15. Peak pitch rate, average power production, and peak rotor speed for rated wind fields; the box plots have lines at the lower quartile, median, and upper quartile values; a solid red line shows the mean (the median is a plotted with a black dotted line); the whiskers extend to the 10th and 90th percentiles; large black dots indicate the extent of the 5th and 95th percentiles; outliers are data with values beyond the dots; each dot is one of the 93 R runs; the larger the number of sample runs, the narrower the notches in the sides of the boxes become; if one box's notches do not vertically overlap with another box's, this indicates with 95% confidence that the true medians of those two boxes do differ

# 5 CART3 Disturbance Feedforward: Individual Blade Pitch using Preview Wind Measurements

## 5.1 Preview Control

Preview control is most readily accomplished in discrete time in which time delays can be modeled as first-order shifts at the sample rate. This study takes the approach outlined in the article by Takaba [18] and augments the linearized, discrete-time plant model with chains of delays as described in Appendix A. This incorporates the delay between the measurement of wind speeds and their arrival at the turbine into the linearized, turbine model in the most straightforward fashion. The contents/measurements stored in the delay chains then are viewed as part of the state of the augmented plant as depicted in Figure 16 for a state-feedback controller. The state-feedback architecture provides a relatively uncomplicated case in which the effect of pitch-rate limitations can be investigated.

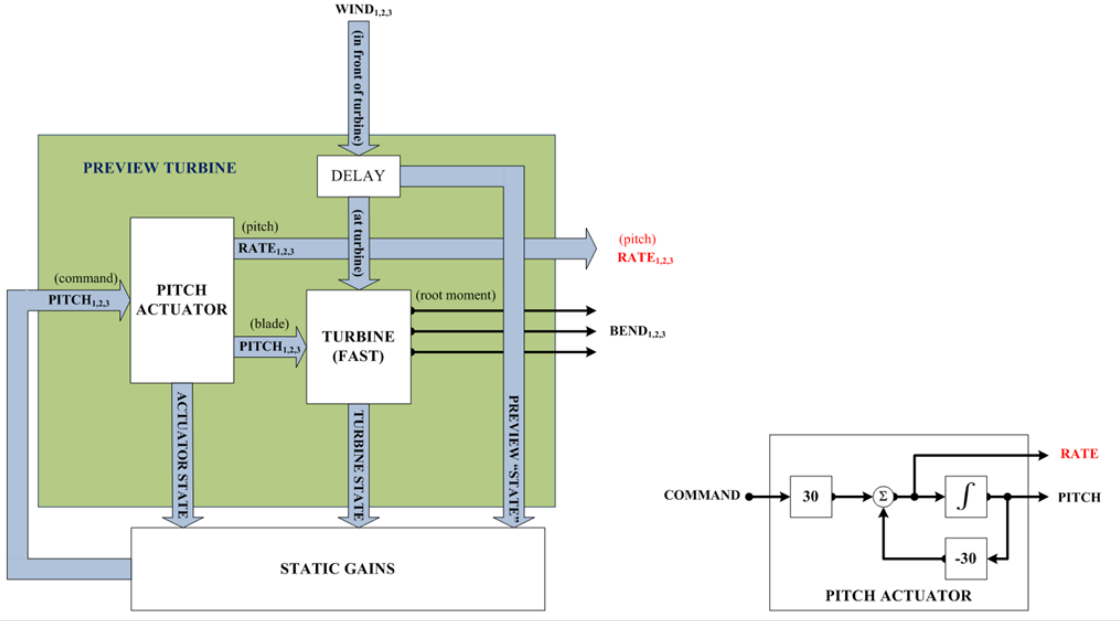


Figure 16. State-feedback, preview controller: (a) linearized turbine augmented with states to model the delay between measured wind and its arrival at the turbine; (b) the complete, linear preview turbine model (green box) incorporates a simple actuator model.

In this configuration the wind measurements are able to effect actuation before the wind impacts the turbine, so this truly is preview control. The design of the state (plant and preview) feedback gains can be accomplished with any desired approach. Without formulating some goal with respect to canceling the effect of the wind at the plant outputs or states, feedback from the preview states is not required (as would be the case for pole placement). Here we minimize the $\mathcal{H}_\infty$ gain (Doyle et al. [19]) from the preview measurements $\mathrm{w}^T(k) = [\mathrm{w}_1(k)\ \mathrm{w}_2(k)\ \mathrm{w}_3(k)]$ to the blade-root bending moments $b_r^T(k) = [b_1(k)\ b_2(k)\ b_3(k)]$ with the additional constraint that the maximum vector pitch rate $\beta_r^T(k) = [\beta_1(k)\ \beta_2(k)\ \beta_3(k)]$ satisfy the following.

$$\max_k \left(\beta_r(k)^T \beta_r(k)\right) \leq \gamma_{e2p}^2 \tag{18}$$

The performance level $\gamma_{e2p}$ is a specified peak magnitude for the pitch-rate vector $\beta_r(k)$ for all wind perturbations $\mathrm{w}(k)$ with total square area bounded by unity.

$$\sum_{k=0}^{\infty} \mathrm{w}(k)^T \mathrm{w}(k) \leq 1 \tag{19}$$

As explained in the book by Skelton, Iwasaki, and Grigoriadis [20] and the article by Scherer, Gahinet, and Chilali [21], there are linear, matrix inequality (LMI) conditions guaranteeing these objectives that can be posed in a form that allows linear programming techniques to be applied. Given a state-space realization for the augmented turbine/actuator/delay system:

$$\begin{aligned} x(k+1) &= A_{sys}\ x(k) + B_{sysw}\ \mathrm{w}(k) + B_{sysp}\ p(k),\ x(0) = 0 \\ \beta_r(k) &= C_{sysr}\ x(k) + D_{sysrw}\ \mathrm{w}(k) + D_{sysrp}\ p(k) \\ b_r(k) &= C_{sysb}\ x(k) + D_{sysbw}\ \mathrm{w}(k) + D_{sysbp}\ p(k) \end{aligned} \tag{20}$$

a state-feedback gain $K$ results in a closed loop satisfying (18) and having $\mathcal{H}_\infty$ gain less than $\gamma_{e2e}$ if there is a positive definite matrix $P$ and a general matrix $G$ satisfying the following two LMIs.

$$\begin{bmatrix} P_{opt} & \star & \star \\ 0 & I_w & \star \\ C_{sysr}P_{opt} + D_{sysrp}G & D_{sysrw} & \gamma_{e2p}^2 I_r \end{bmatrix} > 0 \tag{21}$$

$$\begin{bmatrix} P_{opt} & \star & \star & \star \\ 0 & I_w & \star & \star \\ A_{sys}P_{opt} + B_{sysp}G & B_{sysw} & P_{opt} & \star \\ C_{sysb}P_{opt} + D_{sysbp}G & D_{sysbw} & 0 & \gamma_{e2e}^2 I_m \end{bmatrix} > 0$$

Here, "$\star$" represents the transpose of the corresponding block in the lower part of the matrix and $I_w$, $I_r$, and $I_m$ are identity matrices with dimensions compatible with w, $\beta_r$, and $b_r$, respectively. The second of these inequalities follows quite quickly, starting from the discrete-time bounded real lemma (Vaidyanathan [22]) and a complete proof of the first LMI is given in Skelton et al. [20]. Once solutions $P$ and $G$ are found, a state-feedback gain is given by $K = GP^{-1}$. These inequalities are linear in the variables $P$ and $G$, and solutions can be found using linear programming techniques.

We compute solutions and the minimum achievable $\gamma_{e2e}$ for these LMIs using a linear programming preprocessor YALMIP [23] and the semidefinite-quadratic-linear programming code SDPT3 [24]. Designs are computed for peak pitch-rate magnitudes $\gamma_{e2p}$ from 7.7 to 19 deg/s (slightly greater than the peak rate for the CART3). Again, these are constraints on the magnitude of the pitch-rate

vector, but they correlate fairly well with peak, individual-pitch rates produced by the resulting closed-loop linear model in response to a collective step change in wind speed.

Results are displayed in Figure 17. The plot on the left shows the open (black) and closed-loop (blue-to-red) maximum singular value versus frequency, of the transfer function from wind perturbations to the blade-root bending moments—lower is better. Each closed-loop response shows the result using a different amount of preview as denoted by the color bar on the right (.05 sec to 0.75 sec). The same generous pitch-rate constraint $\gamma_{e2p}$ of 15 deg/s was applied in optimizing each closed loop. As the preview time is increased, the peak, over frequency, of the singular values decreases with the largest improvement having taken place by about 0.40 s of preview. Beyond 0.45 s of preview there is a diminishing return. This also is evident in the plot on the right, which shows the $\mathcal{H}_\infty$ gain achieved versus preview time for a family of pitch-rate constraints as indicated by the color bar on the right (2 deg/s to 19 deg/s). For moderate to aggressive (e.g. $\geq$ 12 deg/s for the CART3) pitch rates, there is very little improvement beyond 0.4 s. of preview. However, if the system is pitch-rate limited (say $\leq$ 8 deg/s), then additional preview beyond 0.75 s (the maximum used in this study) might provide still further decreases in the peak frequency response–though the performance achieved is nowhere near that obtained with greater pitch rates.

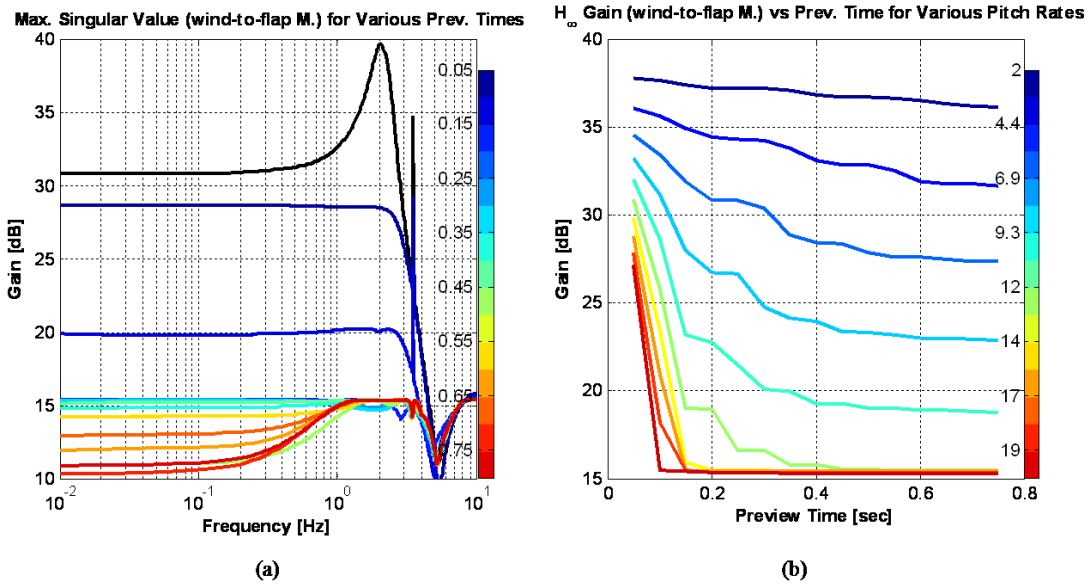


Figure 17. Gain from wind perturbations to perturbations in blade-root, flap-bending moment for pitch-rate constrained, state-feedback preview controllers; (a) closed loop response of MBC based controllers (b) closed loop response of non-MBC controllers.

An important mitigating factor that has not been considered in this study is the frequency range in which reducing the turbine's response to wind disturbance inputs is most beneficial. In particular, no frequency weighting was used in augmenting the turbine model. For the purposes of design, filtering representative of the expected frequency content of wind disturbances could be added at the bending moment outputs in formulating the cost function. The important point being that, in the absence of frequency weighting the limit in achievable performance essentially is set by the high-frequency gain from wind to blade-root bending moment. If little wind energy is expected at these frequencies, then de-emphasizing this range with output weighting could significantly affect the results–particularly where pitch-rate limitations are concerned. Better control (more attenuation)

might be achieved at lower frequencies within the bandwidth of the pitch actuator with appropriate weighting.

## 5.2 Overview of Controllers

The state-feedback controllers explored in the previous section are not realizable, and simply implementing the feedback gains via an observer would not give the same closed-loop frequency response as true state feedback. For this reason, the controllers simulated are designed as dynamic-output feedback controllers but, essentially, the same preview augmentation technique is used in their design as explained in detail in Appendix B. Increasing the amount of preview entails increasing the order of the plant by the number of delays required for the desired preview length and then multiplying this again for each measurement that is previewed. The largest preview we were successfully able to design for was 0.45 s (9 delays) at a controller sample rate of 20 Hz (0.05 s/sample). With three preview wind measurements (one per blade) this translates into an additional 27 states in the plant model– needless to say, these are high-order controllers. Based on the state-feedback study, however, this length of time should be sufficient to gauge the benefits available from preview control.

The controllers are designed using a linearized turbine model from FAST that includes degrees of freedom for the generator inertia, drivetrain compliance, and the first flap mode in each blade as summarized in Table 2. The wind conditions are set to be uniform across the rotor plane at 18 m/s and the generator torque is set to rated, and FAST computes the steady-state response of the turbine and then linearizes the plant at multiple rotor positions. As explained in Appendices A and B, the average linear turbine model is further augmented so that the resulting controllers provide asymptotic rejection of $1P$ bending moments and integral control of rotor speed. To provide a baseline for comparison, we also simulate non-preview collective-pitch (CP) and MBC independent-pitch (IP) controllers as shown in Figure 18. Frequency responses of the baseline controller SISO loops are provided in Appendix B.

The preview controllers are distinguished by several characteristics including that all controller inputs and outputs connect with the same controller-dynamics and that the turbine model is augmented with extra states to incorporate the preview delay. The combined feedforward-feedback compensation is designed simultaneously using the standard, generalized $\mathcal{H}_\infty$ framework (Doyle et al. [19]). This results in a controller of the same order as the complete, augmented plant as depicted in Figures 19(a) and 19(b); no effort to reduce the controller order post-design is made in this study.

FAST computes linearizations of the turbine model with respect to pitch and perturbations $\mathrm{w}_{sh}$ in wind shear, but as shown in Figure 19, the wind measurements are used by the controller either directly as in 19(a) or immediately after the application of the MBC transformation as in 19(b) without computation of shear. This is possible, because prior to design, the coefficients in the linearized model as computed by FAST with respect to shear perturbations are pre-scaled in accordance with (3) or with further application of the MBC-transformation so that the controllers can be based on the direct measurements $[\mathrm{w}_1, \mathrm{w}_2, \mathrm{w}_3]$ of wind speed or their MBC transformed counter parts $[\mathrm{w}_u, \mathrm{w}_c, \mathrm{w}_s]$. Details are given in Appendix A.

The preview controllers are optimized so that there are two controllers for each of the MBC and

Table 4. CART3 Controller Summary

| Controller | | Max. RMS pitch rate [deg/sec] | Preview Time [sec] | Augmentation | Order |
|---|---|---|---|---|---|
| MBC | MBCPrev | 10.1 | 0.45 | DC speed error<br>1P vertical / horizontal bending moments | 47 |
| | | 7.1 | | | |
| | IP | 5.76 | none | | 5 |
| non-MBC | Prev | 11.57 | 0.45 | DC speed error<br>1P bending moments | 55 |
| | | 7.4 | | | |
| | CP | 1.26 | none | DC speed error | 3 |

non-MBC preview cases with moderate and slightly aggressive rms pitch rates as summarized in Table 4. Including the baseline controllers, this makes a total of six designs used in performance simulations. For comparison, the maximum singular value of the transfer function from wind perturbation to blade-root bending moment are shown in Figure 20 for the MBC controllers (on the left) and the non-MBC controllers (on the right). The intention was to have comparable control effort (as characterized by rms pitch rate) between the MBC and non-MBC cases, but the MBC controllers inadvertently were weighted for slightly better speed regulation. The non-MBC designs contain augmented dynamics to reject $1P$ bending moments and this is evident in the notch at 0.7 Hz (41.7 rpm). The MBC designs were augmented to achieve similar rejection, but because of the MBC transformation, these controllers see $1P$ variation as a DC disturbance in the vertical and horizontal components and so they are designed/augmented to have asymptotic rejection at 0 Hz. Note in both MBC and non-MBC cases, the amount of attenuation in the peak gain, over all frequencies, is better with larger pitch rates and that the peaks achieved are comparable between MBC and non-MBC preview controllers. The baseline, feedback-only controllers have significantly higher peaks.

## 5.3 Simulation Results

The six controllers are simulated in each of the 93 wind realizations obtained from TurbSim, described under CART3 in Table 0.2. In every case, all degrees of freedom for the turbine model provided by FAST were enabled even though the controllers were designed for a reduced set of DOFs (see Table 2). The preview controllers are simulated twice in each wind condition. One simulation uses the rotating measurement scheme and the second uses wind speeds interpolated from stationary measurements. Recall that, when using stationary measurements, after MBC transforming the individual stationary measurements the MBC controller uses the results directly, but the results must be interpolated for use with the non-MBC controller. The inaccuracy inherent in the stationary measurements still affects MBC and non-MBC controllers with the same degradation in performance. In either case, the measurements must reflect conditions local to the blades; the shear (or equivalent MBC) components experienced by the blades can be significantly different than those measured at the stationary locations.

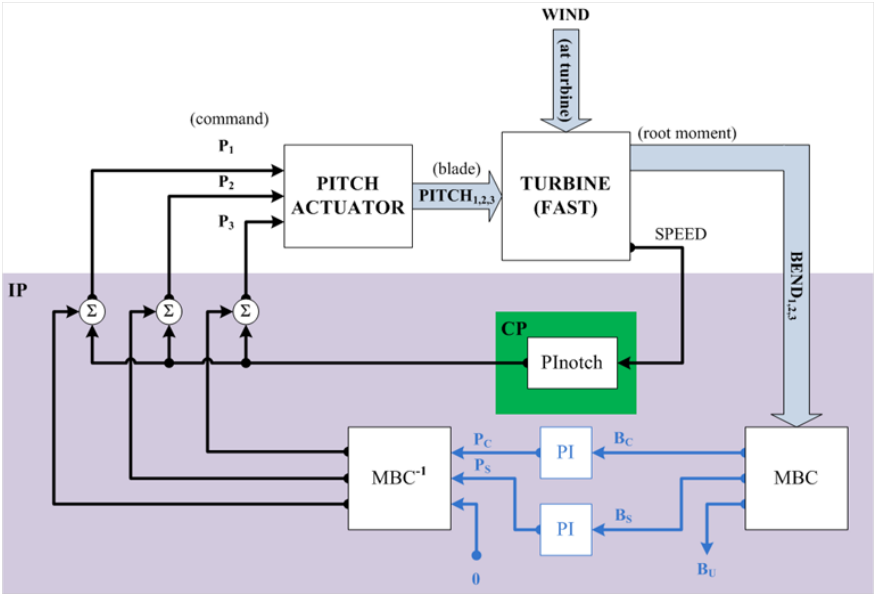


Figure 18. Baseline controllers: collective-pitch controller (green); in implementation, the MBC path is absent during CP simulation whereas all blocks are in place during simulation of the MBC IP controller.

Box plots of the results for pitch rate, generator power, and blade-root bending moment in the flap direction are provided in Figure 21 using data from all 93 simulations. The box indicates the median (notch center), mean (red belt), and first quartiles (box ends) from the median. The whiskers denote 5% and 95%, and the dots show outliers. When using rotating measurements, the preview controllers provide significant performance improvements when compared with the feedback-only collective-pitch (CP) and independent pitch (IP) baseline controllers. When using stationary measurements, however, the performance of the preview controllers degrades to less than that of the IP feedback-only controller.

Damage equivalent loads are computed for blade-root bending moment and tower-base bending moment in the fore-aft and side-to-side directions. The RMS tower sway is also computed in the fore-aft and side-to-side directions. The percent change for each controller relative to the IP feedback-only baseline controller is indicated in the bar charts of Figure 22. The first controller on the left in both charts is the CP feedback-only controller, which has the same performance independent of the preview measurement technique (as does the baseline IP controller). All the metrics are defined so that lower always is better.

As long as measurements accurately reflect conditions local to the blades (rotating measurements, left chart) relative to baseline, preview control provides significant improvement in the root-flap moment (dark blue) which the controllers were designed to mitigate. In particular, the use of preview control decreases loading by more than 20%. When there are errors in wind measurements (stationary measurements, right chart), the preview performance in the flap-moment metric increases loading by more than 10% in some cases.

The controllers are not designed to mitigate tower motion but, in the case of tower side-to-side motion, blade flap *appears* to be correlated in such a way that mitigation of root loads also reduces

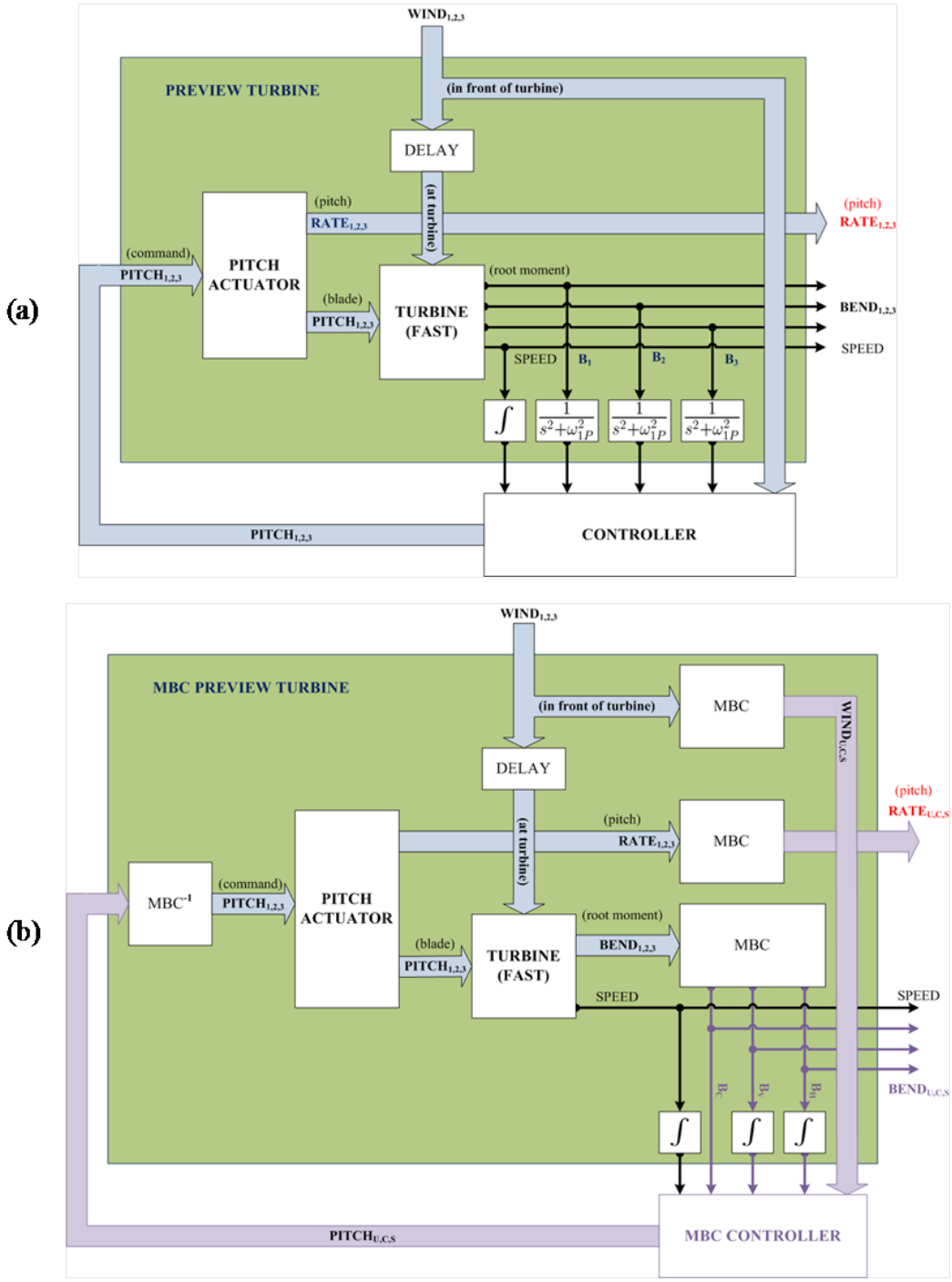


Figure 19. Dynamic output feedback, preview controllers: (a) non-MBC controller; (b) MBC controller.

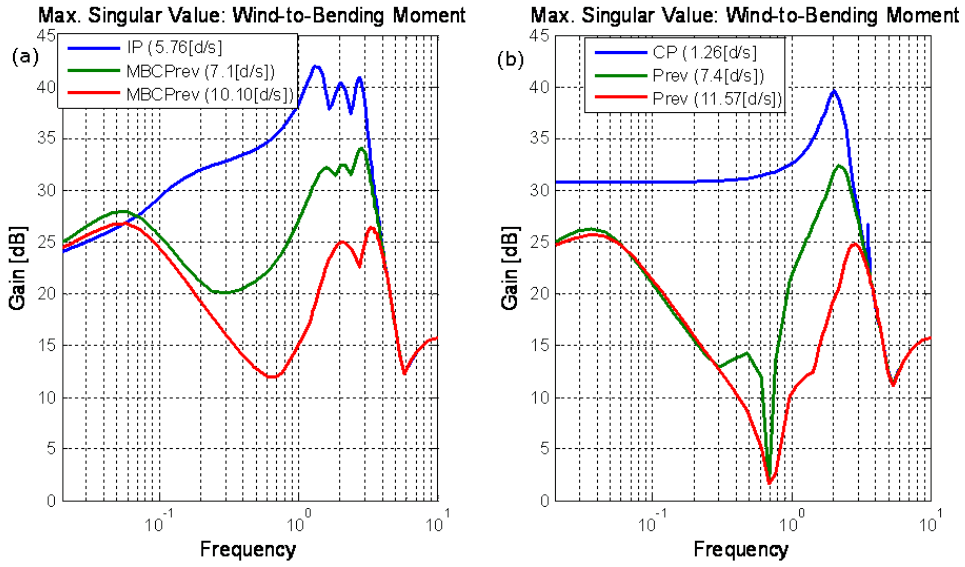


Figure 20. Gain from perturbations in wind to perturbations in blade-root, flap-bending moment for several amounts of preview: (a) MBC preview controllers; (b) non-MBC controllers.

side-side loading. Somewhat unexpectedly, the use of preview results in significantly worse performance than feedback-only with respect to tower loads in the fore-aft direction (green bars). It is unclear why decreasing flap loads should not also decrease fore-aft tower loading.

Overall, the potential performance improvements with preview control are significant. In order to realize these advantages careful consideration of the shortcomings in the measurement system and the expected frequency content of the wind must be taken into account during design. As explained in the overview of the controllers, in this study no special consideration was made with respect to either of these factors–this is a topic for future work.

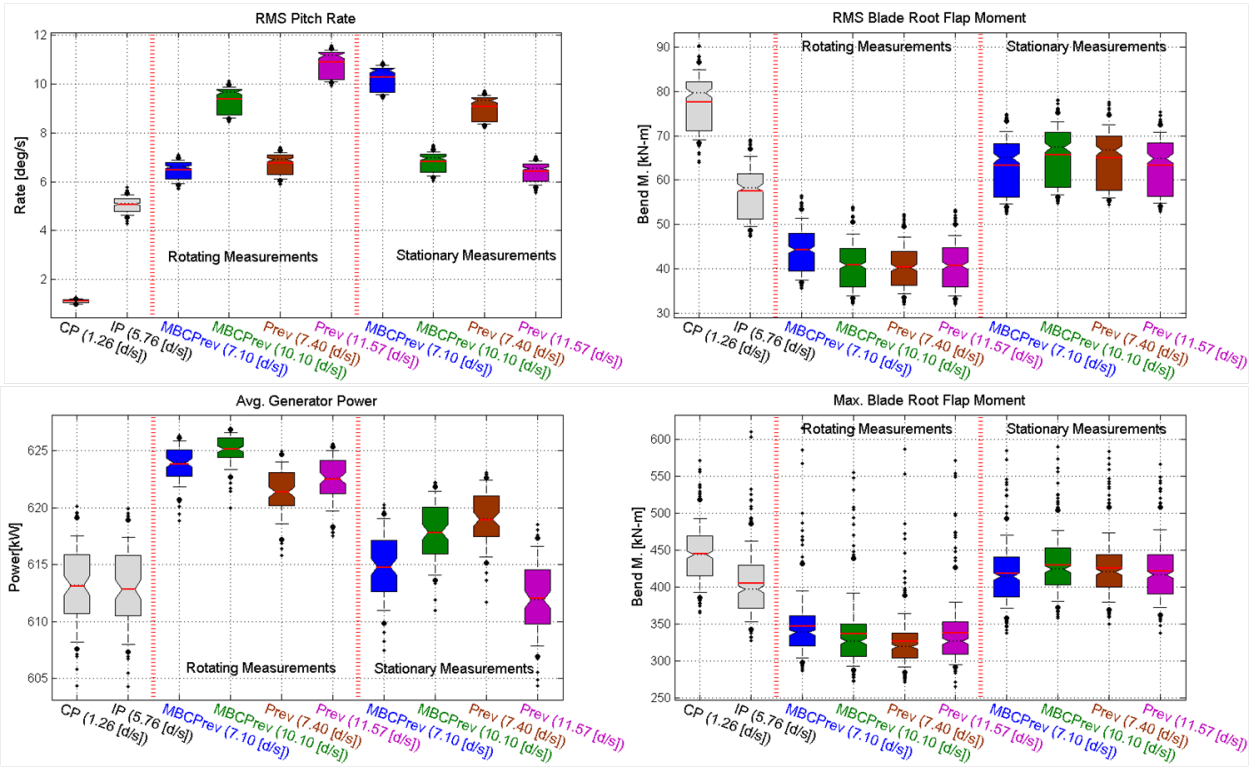


Figure 21. Summary of results for all 93 simulations: top left— rms pitch rate; lower left— average generator power; top right— rms blade-root bending moments; lower right— maximum blade-root, flap-bending moment.

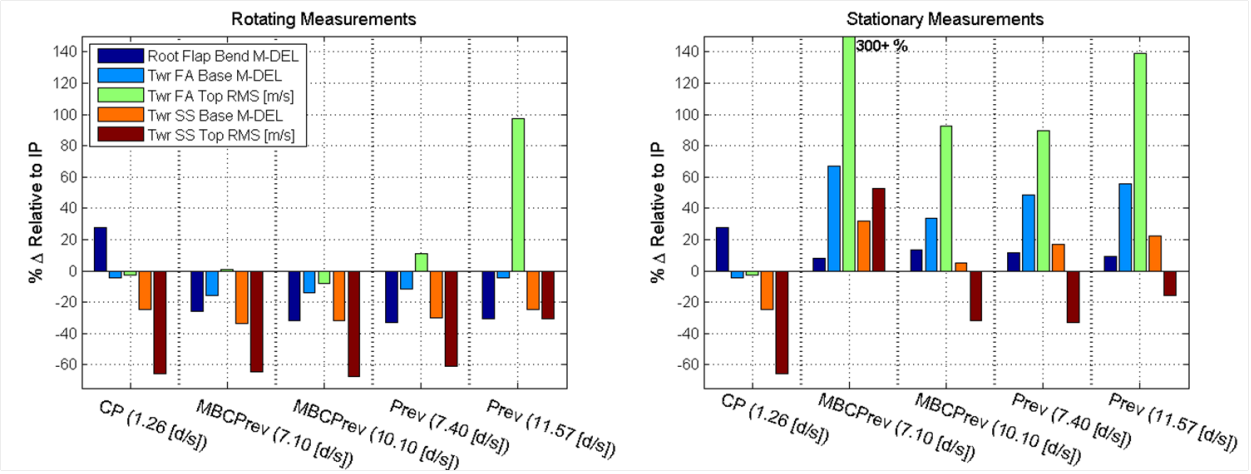


Figure 22. Load Metrics relative to feedback-only, independent pitch (IP): left plot— percent increase relative to baseline using rotating measurements; right— percent increase relative to baseline using stationary measurements.

# 6 Discussion, Conclusions, and Future Work

## 6.1 Conclusions on Controller Studies for the 5-MW Turbine

This report presents results of an initial study of feedforward blade-pitch control when added to standard feedback control. Two baseline feedback controllers, three collective-pitch feedforward controllers, and five individual pitch feedforward controllers were designed. Various combinations of these feedback and feedforward controllers were evaluated on a nonlinear 5-MW wind turbine model using realistic wind fields representative of the Great Plains region in the United States, with above-rated and rated wind conditions. A method for phasing out individual pitch control as wind speeds become less than rated also was developed.

For collective-pitch feedforward controllers with no preview, three possible wind-speed inputs were compared. An average of wind-speed measurements over five points in space performed much better than a single hub-height-only wind-speed measurement. It appears, however, that the best input would not come from either of these LIDAR-based methods, but instead from a wind-speed estimate based only on generator speed, generator torque, and blade pitch—but such estimates cannot provide preview wind estimates.

When the collective-pitch feedback baseline controller is augmented with any of the collective-pitch feedforward controllers, the overall performance (in terms of loads and power production) is worse than when using the collective-pitch feedback baseline controller alone.

Two of the shaped individual-pitch feedforward controllers (IP shaped 5 s feedforward and IP shaped 10/3 s feedforward) show an improvement better than the individual-pitch feedback-only baseline. The optimal preview time was between 3 s and 5 s, but this is specific to the shaped controller design and might not be true in general.

Future work includes investigating other types of feedforward control approaches, including non-causal series expansion (Gross et al. [25]) and Preview Control (Tomizuka et al. [26]) techniques. These methods allow for a varying preview time, which is advantageous because—due to various hardware implementation issues—it is preferable for LIDARs to be set to measure wind speeds from a fixed distance away. Therefore, the available preview time will vary as the wind speed varies. A non-causal series expansion is a model-inverse method that might be superior to those presented in this report because it can utilize longer preview times. Preview Control includes a cost function that allows explicit minimization of rotor-speed error, loads, and pitch rate.

## 6.2 Conclusions on Controller Studies for CART3

For this study, preview controllers were designed and compared against baseline non-preview collective-pitch and independent-pitch controllers for load mitigation in above-rated wind conditions. The controllers were augmented to provide integral control of rotor/generator speed and asymptotic rejection of $1P$ variations in blade-root bending moments. This biased the controllers to mitigate these specific narrow-band disturbances but, otherwise, no weighting or foreknowledge of wind-frequency content or of measurement characteristics was brought to bear in the design.

The results show that preview control can provide significant improvements in load mitigation.

The amount of improvement, however, is directly affected by available pitch rate and the accuracy of wind measurements. In turbulent conditions where shear is not uniform, the use of preview measurements that do not reflect conditions local to each blade actually can reduce performance to less than that attained using control based only on feedback of turbine measurements. It appears that the amount of deterioration is dependent on the aggressiveness of the controller and the frequency range in which measurements provide the best accuracy. Even the simple interpolation scheme of the stationary measurements that is used in this study retained some accuracy at lower frequencies in turbulent conditions.

Originally, we thought that MBC might provide some insulation against measurement errors because it is based on non-rotating components of blade variables. In particular, it was hoped that MBC might work well with the much simpler stationary measurements. Results show that this is not the case. In turbulent conditions, the "local" shear or equivalent MBC components of the wind can vary significantly as the blades are positioned within the rotor disk at different azimuths.

Simulation results show that without further consideration, handling of measurements, or optimization of the controller to account for the errors that simpler measurement schemes can produce, the advantages of wind measurements can be greatly diminished. When conditions become turbulent enough, as in the CART3 simulation conditions, it might be better to stop using preview control when using measurement techniques that are less accurate than the rotating scheme. This turned out to be the case for both MBC and non-MBC controllers. In more uniform less turbulent conditions, however, we still expect that the use of measurements simpler than a rotating scheme can be beneficial for both MBC and non-MBC controllers. Further, when wind variation largely is due to linear shear and uniform perturbations, MBC can provide a significant advantage in that the rejection of $1P$ variation in bending moments can be accomplished independent of rotor speed and with simpler controller dynamics.

The sensitivities to measurement error in turbulent conditions might be mitigated by more effort in three areas.

- Controller optimization should take into account the expected spectral content of wind disturbances.
- If it is known that the wind measurements have poor accuracy within certain frequency ranges (e.g., high frequencies), then at least the feedforward section of the controller response should be muted at these frequencies to avoid actuation in response to noise.
- The controller effort and, if possible, measurements should be matched to the available actuator bandwidth.

This study took into account actuator limitations only by weighting pitch rate during optimization to attain reasonable pitch rates. Other than specific augmentations to achieve rejection of DC speed errors and $1P$ bending moments, the controllers were not optimized to address any specific frequency range. As a result, the amount of attenuation achieved essentially was determined by the response of the turbine at higher frequencies. We expect that better performance and perhaps less sensitivity to measurement error can be attained by weighting the performance objective to de-emphasize higher frequencies. If the majority of wind energy is within the bandwidth of the actuator, then in the presence of measurement errors it still might be possible to retain much of the performance gain achieved with ideal measurements.

## 6.3 Overall Conclusions

Disturbance feedforward blade-pitch controllers were designed and simulated for both the 5-MW and CART3 wind turbine models. Blade and tower loads were reduced by more than 10% in the best 5-MW designs. In CART3 designs, blade loads were reduced by more than 30%, and tower loads were reduced by more than 10%. Load reductions are stated relative to an individual-pitch feedback-only baseline control, which itself is 20% to 30% better than industry standard collective-pitch feedback-only control in terms of blade-root loads. These simulation results show that, given an accurate preview of the wind speeds that will hit the turbine blades, a significant reduction in wind turbine structural loads can be achieved.

## References


1. Jonkman, J., Butterfield, S., Musial, W., and Scott, G. *Definition of a 5-MW Reference Wind Turbine for Offshore System Development.* National Renewable Energy Laboratory, Golden, CO, Feb. 2009.

2. Jonkman, J.M. and Buhl, M. L. *FAST User's Guide.* National Renewable Energy Laboratory, Golden, CO, 2005.

3. Kelley, N. D. and Jonkman, B. J. *Overview of the Turbsim Stochastic Inflow Turbulence Simulator: Version 1.21 (Revised Feb. 1, 2007).* National Renewable Energy Laboratory, Golden, CO, April 2007.

4. Pao, L. and Johnson, K. "A tutorial on the dynamics and control of wind turbines and wind farms." In "Proceedings of the American Controls Conference," pages 2076–2089. St. Louis, MO, June 2009.

5. Laks, J. H., Pao, L. Y., and Wright, A. "Combined feedforward/feedback control of wind turbines to reduce blade flap bending moments." In "Proceedings AIAA/ASME Wind Energy Symposium," pages 82–86. Orlando, FL, Jan. 2009.

6. Bossanyi, E. A. "Individual blade pitch control for load reduction." *Wind Energy*, 6:119–128, 2003.

7. Bir, G. *Multiblade Coordinate Transformation and Its Application to Wind Turbine Analysis.* National Renewable Energy Laboratory, Golden, CO, 2008.

8. Laks, J. H., Dunne, F., Wang, N., Pao, L. Y., Johnson, K. E., Wright, A. G., Frehlich, R. G., Jonkman, B., and Kelley, N. "Feasibility studies on disturbance feedforward techniques and tower and blade feedback to improve load mitigation performance." report for industrial sponsor, 2010.

9. Østergaard, K.Z., Brath, P., and Stoustrup, J. "Estimation of effective wind speed." *Journal of Physics: Conference Series 75: The Science of Making Torque from Wind*, 2007.

10. Schlipf, David, Trujillo, Juan J., Basterra, Valeria, and Kühn, Martin. "Development of a wind turbine lidar simulator." In "Proceedings of the European Wind Energy Conference," Parc Chanot, Marseille, France, March 2009.

11. Harris, M., Hand, M., and Wright, A. *Lidar for Turbine Control.* National Renewable Energy Laboratory, Golden, CO, 2006.

12. Stol, K. and Fingersh, L. "Wind turbine field testing of state-space control designs." In "NREL/SR-500-35061," 2004.

13. Wright, A., Stol, K., and Fingersh, L. "Progress in implementing and testing state-space controls for the controls advanced research turbine." In "24th ASME Wind Energy Conference," pages 88–100. Reno, NV, 2005.

14. Stol, K., Zhao, W., and Wright, A. "Individual blade pitch control for the controls advanced research turbine (cart)." *ASME J. Solar Energy Engineering*, 128(4):498–505, November 2006.

15. *Simulation and Model-Design Software Package.* The MathWorks, Inc., Natick, MA.

16. Butterworth, J.A., Pao, L.Y., and Abramovitch, D.Y. "The effect of nonminimum-phase zero locations on the performance of feedforward model-inverse control techniques in discrete-time systems." In "Proc. American Control Conference," pages 2696–2702. Seattle, WA, 2008.

17. Downing, S. D. and Socie, D. F. "Simple rainflow counting algorithms." *International Journal of Fatigue*, 4(1):31–40, Jan. 1982.

18. Takaba, K. "A tutorial on preview control systems." In "SICE Annual Conference," Fukui University, Japan, Aug. 2003.

19. Doyle, J.C., Glover, K., Khargonekar, P.P., and Francis, B.A. "State-space solutions to standard $\mathcal{H}_\infty$ and $\mathcal{H}_2$ control problems." *IEEE Transactions on Automatic Control*, 34(8):831–847, Aug. 1989.

20. Skelton, Robert E., Iwasaki, T., and Grigoriadis, Karolos M. *A Unified Algebraic Approach To Control Design*. Taylor & Francis Inc., Bristol, PA, 1st edition, Oct. 1997.

21. Scherer, C., Gahinet, P., and Chilali, M. "Multiobjective output-feedback control via lmi optimization." *IEEE Transactions on Automatic Control*, 42(7):896–911, July 1997.

22. Vaidyanathan, P.P. "The discrete-time bounded-real lemma in digital filtering." *IEEE Transactions on Circuits and Systems*, 32(9), 1985.

23. Löfberg, J. "YALMIP: A toolbox for modeling and optimization in MATLAB." In "Proceedings of the CACSD Conference," Taipei, Taiwan, 2004.

24. Kim-Chuan Toh, Michael J. Todd and Tutuncu, Reha H. "A matlab software for semidefinite-quadratic-linear programming, version 4.0 (beta)."

25. Gross, E. and Tomizuka, M. "Experimental flexible beam tip tracking control with a truncated series approximation to uncancelable inverse dynamics." *IEEE Trans. Ctrl. Sys. Tech.*, 2(4), Dec. 1994.

26. Tomizuka, M. and Fung, D.H. "Design of digital feedforward/preview controllers for processes with predetermined feedback controllers." *ASME J. Dyn. Sys., Meas. & Ctrl.*, 102:218–225, Dec. 1980.

27. Franklin, Gene F., Powell, J. David, and Workman, Michael. *Digital Control of Dynamic Systems*. Addison-Wesley, 3rd edition, 1997.

28. Francis, B. A. *A Course in $\mathcal{H}_\infty$ Control Theory, Lecture Notes in Control and Information Sciences, Vol. 88.* Springer-Verlag, 1987.

# Appendix

# A CART3 Turbine Models

## A1 CART3 Non-MBC Turbine Model

The starting point for obtaining a turbine model is simulation and linearization using FAST at rated speed and torque. The salient features of the CART3 are summarized in Tables 1 and 2. The wind speed is set to 18 m/s uniform and FAST simulates the turbine to find periodic operating conditions; then FAST linearizes the turbine at a number of equally spaced rotor azimuths. We then use these linearizations to obtain an average state-space model.

A linearized state-space model of the turbine

$$\begin{array}{rcl} \dot{x}_p & = & A_F(\theta)x_p + [B_{Fsh}(\theta)\ B_{F\beta}(\theta)] \begin{matrix} \mathrm{w}_{sh} \\ \beta \end{matrix} \\ \begin{matrix} b_r \\ \Omega_g \end{matrix} & = & \begin{matrix} C_{Fb}(\theta) \\ C_{Fg}(\theta) \end{matrix} x_p + \begin{matrix} D_{Fbsh}(\theta) & D_{Fbp}(\theta) \\ D_{Fgsh}(\theta) & D_{Fgp}(\theta) \end{matrix} \begin{matrix} \mathrm{w}_{sh} \\ \beta \end{matrix}, \end{array} \tag{A1}$$

is obtained from FAST at rotor azimuth $\theta$ where $x_p^T = [x_t^T, x_r^T, v_r^T]$ contains states representing the turbine fixed-frame degrees of freedom (DOF) and blade displacements $x_r$ and velocities $v_r$. We augment this system with three, parallel, first-order, actuator models (see Figure 16)

$$\begin{array}{rcl} \dot{x}_{ar} & = & A_{ar}\ x_{ar} + B_{ap}\ p \\ \begin{matrix} \beta \\ \beta_r \end{matrix} & = & \begin{matrix} C_{ap} \\ C_{apr} \end{matrix} x_{ar} + \begin{matrix} D_{ap} \\ D_{apr} \end{matrix} p, \end{array} \tag{A2}$$

where $\beta^T = [\beta_1, \beta_2, \beta_3]$ contains the pitch of each blade achieved by the actuators, $\beta_r$ contains the associated pitch rates and

$$\begin{array}{ll} A_{ar} = -30 \cdot I_{3\times 3} & B_{ap} = 30 \cdot I_{3\times 3} \\ C_{ap} = I_{3\times 3} & D_{ap} = 0 \cdot I_{3\times 3} \\ C_{apr} = -30 \cdot I_{3\times 3} & D_{apr} = 30 \cdot I_{3\times 3}. \end{array} \tag{A3}$$

This system of actuators is then combined with the FAST linearization to get a composite state-space system

$$\begin{array}{rcl} \dot{x} & = & \begin{matrix} A_F(\theta) & B_{F\beta}(\theta)\ C_{ap} \\ 0 & A_{ar} \end{matrix} x + \begin{matrix} B_{Fsh}(\theta) & B_{F\beta}(\theta)\ D_{ap} \\ 0 & B_{ar} \end{matrix} \begin{matrix} \mathrm{w}_{sh} \\ p \end{matrix} \\ \begin{bmatrix} \Omega_g \\ b_r \\ \beta_r \end{bmatrix} & = & \begin{bmatrix} C_{Fg}(\theta) & D_{Fgp}(\theta)\ C_{ap} \\ C_{Fb}(\theta) & D_{Fbp}(\theta)\ C_{ap} \\ 0 & C_{apr} \end{bmatrix} x + \begin{bmatrix} D_{Fgsh}(\theta) & D_{Fgp}(\theta)D_{ap} \\ D_{Fbsh}(\theta) & D_{Fbp}(\theta)D_{ap} \\ 0 & D_{apr} \end{bmatrix} \begin{matrix} \mathrm{w}_{sh} \\ p \end{matrix}, \end{array} \tag{A4}$$

or more simply

$$\begin{aligned} \dot{x} &= A(\theta)x + [B_{sh}(\theta)\ B_p(\theta)] \begin{matrix} \mathrm{w}_{sh} \\ p \end{matrix} \\ \begin{bmatrix} \Omega_g \\ b_r \\ \beta_r \end{bmatrix} &= \begin{bmatrix} C_g(\theta) \\ C_b(\theta) \\ C_r(\theta) \end{bmatrix} x + \begin{bmatrix} D_{gsh}(\theta) & D_{gp}(\theta) \\ D_{bsh}(\theta) & D_{bp}(\theta) \\ D_{rsh}(\theta) & D_{rp}(\theta) \end{bmatrix} \begin{matrix} \mathrm{w}_{sh} \\ p \end{matrix} , \end{aligned} \tag{A5}$$

where $x^T = [x_t^T, x_r^T, v_r^T, x_{ar}^T]$.

The only change we wish to make in this model for non-MBC design purposes is to have input coefficients which are relative to equivalent blade local wind perturbations (and will have corresponding preview measurements). Recall (Section 3 equations (3) and (4)) that if the wind perturbation consists of only uniform and shear components, then a transformation from the equivalent individual perturbations to the shear perturbations used by FAST is given by

$$\mathrm{w}_{sh} = M_{m2s} T(\theta)^{-1} \mathrm{w}_t, \tag{A6}$$

where the conversion $M_{m2s}$ from MBC to shear perturbations and the basic MBC transform $T(\theta)^{-1}$ are defined in equations (3) and (4), respectively. Here the wind input is denoted $\mathrm{w}_t^T = [\mathrm{w}_{t1}, \mathrm{w}_{t2}, \mathrm{w}_{t3}]$ to emphasize that this is the wind at the 75% span of each turbine blade; $\mathrm{w}^T = [\mathrm{w}_1, \mathrm{w}_2, \mathrm{w}_3]$ is now reserved for the measurements out in front of the turbine.

Now, a state-space model with input coefficients relative to perturbations in individual wind measurements is obtained by substituting (A6) into (A5) to obtain

$$\begin{aligned} \dot{x} &= A(\theta)x + [B_{sh}(\theta)\ B_p(\theta)] \begin{matrix} M_{m2s}T(\theta)^{-1} & 0 & \mathrm{w}_t \\ 0 & I & p \end{matrix} \\ \begin{bmatrix} \Omega_g \\ b_r \\ \beta_r \end{bmatrix} &= \begin{bmatrix} C_g(\theta) \\ C_b(\theta) \\ C_r(\theta) \end{bmatrix} x + \begin{bmatrix} D_{gsh}(\theta) & D_{gp}(\theta) \\ D_{bsh}(\theta) & D_{bp}(\theta) \\ D_{rsh}(\theta) & D_{rp}(\theta) \end{bmatrix} \begin{matrix} M_{m2s}T(\theta)^{-1} & 0 & \mathrm{w}_t \\ 0 & I & p \end{matrix} , \end{aligned} \tag{A7}$$

or simply

$$\begin{aligned} \dot{x} &= A(\theta)x + [B_w(\theta)\ B_p(\theta)] \begin{matrix} \mathrm{w}_t \\ p \end{matrix} \\ \begin{bmatrix} \Omega_g \\ b_r \\ \beta_r \end{bmatrix} &= \begin{bmatrix} C_g(\theta) \\ C_b(\theta) \\ C_r(\theta) \end{bmatrix} x + \begin{bmatrix} D_{gw}(\theta) & D_{gp}(\theta) \\ D_{bw}(\theta) & D_{bp}(\theta) \\ D_{rw}(\theta) & D_{rp}(\theta) \end{bmatrix} \begin{matrix} \mathrm{w}_t \\ p \end{matrix} . \end{aligned} \tag{A8}$$

Then, an average state-space system is obtained from the complete set of linearizations (A8) at $N$ azimuth angles $\theta_i$ by computing, for example

$$A = \frac{1}{N}\sum_{i=1}^{N} A(\theta_i). \tag{A9}$$

## A2 CART3 MBC Turbine Model

The MBC transform is used on each degree of freedom (DOF) that rotates with the turbine blades as a function of azimuth $\theta$. Loosely speaking, the transform computes the cosine and sine coefficients of the $1P$ variation in the rotating variables. The basic transform is defined in terms of displacements; each DOF that rotates with or is inherently part of a blade has a displacement/state $x_i$. The goal is to express the differential equation (A5) for the linear system in states/coordinates that do not rotate with the blades. This is accomplished by expressing the rotating states as a function of their MBC/non-rotating counter parts. The rotating state $x_r$ is given by the inverse MBC transform of corresponding non-rotating components $x_{nr}^T = [x_u, x_c, x_s]$ according to

$$x_r \quad = \quad T(\theta)x_{nr}. \tag{A10}$$

Each DOF in a mechanical system also has an associated velocity $v_i = \dot{x}_i$ which requires computation of

$$\dot{x}_r = \dot{T}(\theta)\Omega\ x_{nr} + T(\theta)\dot{x}_{nr}, \tag{A11}$$

where $\Omega = \dot{\theta}$ is the rotor speed. So, the second-order transformation to the rotating DOFs is given by

$$\begin{matrix} x_r \\ v_r \end{matrix} \quad = \quad \begin{matrix} T(\theta) & 0 & x_{nr} \\ \dot{T}(\theta)\Omega & T(\theta) & v_{nr} \end{matrix} \tag{A12}$$

where $v_{nr} = \dot{x}_{nr}$ and

$$\dot{T}(\theta) = \begin{bmatrix} 0 & -\sin(\theta) & \cos(\theta) \\ 0 & -\sin(\theta + \frac{2\pi}{3}) & \cos(\theta + \frac{2\pi}{3}) \\ 0 & -\sin(\theta + \frac{4\pi}{3}) & \cos(\theta + \frac{4\pi}{3}) \end{bmatrix}. \tag{A13}$$

This transformation must be replicated for each rotating degree of freedom. For the sake of simplicity, we assume there is only one rotating DOF in the turbine model, but we add the three, parallel, first-order models of the pitch actuators that rotate with the blades. Including these as part of the rotating system requires that we modify the transformation to

$$\begin{bmatrix} x_r \\ v_r \\ x_{ar} \end{bmatrix} = \begin{bmatrix} T(\theta) & 0 & 0 \\ \dot{T}(\theta)\Omega & T(\theta) & 0 \\ 0 & 0 & T(\theta) \end{bmatrix} \begin{bmatrix} x_{nr} \\ v_{nr} \\ x_{anr} \end{bmatrix}, \tag{A14}$$

where $x_{ar}$ contains the pitch angles produced by the three actuators and $x_{anr}$ contains the uniform, cosine and sine components of the pitch in the non-rotating frame. This completes the transformation between non-rotating and rotating states. Now, recalling that all the other (non-rotating) turbine states are lumped into the vector $x_t$, the complete (non-dynamic) MBC state transformation is given by

$$\begin{aligned}\begin{bmatrix} x_t \\ x_r \\ v_r \\ x_{ar} \end{bmatrix} &= \begin{bmatrix} I & 0 & 0 & 0 \\ 0 & T(\theta) & 0 & 0 \\ 0 & \dot{T}(\theta)\Omega & T(\theta) & 0 \\ 0 & 0 & 0 & T(\theta) \end{bmatrix} \begin{bmatrix} x_t \\ x_{nr} \\ v_{nr} \\ x_{anr} \end{bmatrix} \\ x &= M(\theta)\hat{x}. \end{aligned} \tag{A15}$$

We now make use of (A15) to derive the state-space representation of the linear differential equation in non-rotating/MBC coordinates. This is accomplished by first taking the time derivative of both sides of (A15),

$$\begin{aligned}\begin{bmatrix} \dot{x}_t \\ \dot{x}_r \\ \dot{v}_r \\ \dot{x}_{ar} \end{bmatrix} &= \begin{bmatrix} 0 & 0 & 0 & 0 \\ 0 & \dot{T}(\theta)\Omega & 0 & 0 \\ 0 & \ddot{T}(\theta)\Omega^2 + \dot{T}(\theta)\Omega\dot{\Omega} & \dot{T}(\theta)\Omega & 0 \\ 0 & 0 & 0 & \dot{T}(\theta)\Omega \end{bmatrix} \begin{bmatrix} x_t \\ x_{nr} \\ v_{nr} \\ x_{anr} \end{bmatrix} + \begin{bmatrix} I & 0 & 0 & 0 \\ 0 & T(\theta) & 0 & 0 \\ 0 & \dot{T}(\theta)\Omega & T(\theta) & 0 \\ 0 & 0 & 0 & T(\theta) \end{bmatrix} \begin{bmatrix} \dot{x}_t \\ \dot{x}_{nr} \\ \dot{v}_{nr} \\ \dot{x}_{anr} \end{bmatrix} \\ &= \begin{bmatrix} 0 & 0 & 0 & 0 \\ 0 & \dot{T}(\theta)\Omega & 0 & 0 \\ 0 & \ddot{T}(\theta)\Omega^2 & 2\dot{T}(\theta)\Omega & 0 \\ 0 & 0 & 0 & \dot{T}(\theta)\Omega \end{bmatrix} \begin{bmatrix} x_t \\ x_{nr} \\ v_{nr} \\ x_{anr} \end{bmatrix} + \begin{bmatrix} I & 0 & 0 & 0 \\ 0 & T(\theta) & 0 & 0 \\ 0 & 0 & T(\theta) & 0 \\ 0 & 0 & 0 & T(\theta) \end{bmatrix} \begin{bmatrix} \dot{x}_t \\ \dot{x}_{nr} \\ \dot{v}_{nr} \\ \dot{x}_{anr} \end{bmatrix} \\ \dot{x} &= \bar{M}(\theta)\hat{x} + M_d(\theta)\frac{d}{dt}\hat{x}, \end{aligned} \tag{A16}$$

where

$$\ddot{T}(\theta) = \begin{bmatrix} 0 & -\cos(\theta) & -\sin(\theta) \\ 0 & -\cos(\theta + \frac{2\pi}{3}) & -\sin(\theta + \frac{2\pi}{3}) \\ 0 & -\cos(\theta + \frac{4\pi}{3}) & -\sin(\theta + \frac{4\pi}{3}) \end{bmatrix}, \tag{A17}$$

and simplifications (to get the diagonal matrix $M_d(\theta)$) are obtained by assuming $\dot{\Omega} = 0$ and utilizing the fact that $\dot{x}_{nr} = v_{nr}$. Equating this result with the right hand side of (A5), substituting in (A15) for $x$ and solving for the time derivative of $\hat{x}$ gives

$$
\begin{aligned}
\frac{d}{dt}\hat{x} &= M_d(\theta)^{-1} \;\; A(\theta)M(\theta) - \bar{M}(\theta) \;\; \hat{x} + M_d^{-1}(\theta)[B_{sh}(\theta) \; B_p(\theta)] \begin{matrix} \mathrm{w}_{sh} \\ p \end{matrix} \qquad \text{(A18)} \\
\frac{d}{dt}\hat{x} &= M_d(\theta)^{-1} \;\; A(\theta)M(\theta) - \bar{M}(\theta) \;\; \hat{x} + M_d^{-1}(\theta)[B_{sh}(\theta) \; B_p(\theta)] \begin{matrix} M_{m2s} & 0 & \mathrm{w}_{mbc} \\ 0 & T(\theta) & p_{nr} \end{matrix} \\
&= A_{MBC}(\theta)\hat{x} + [B_{wMBC}(\theta) \; B_{cMBC}(\theta)] \begin{matrix} \mathrm{w}_{mbc} \\ p_{nr} \end{matrix} \;\; ,
\end{aligned}
$$

where we have used the conversion $M_{m2s}$ from MBC wind components to shear wind components that was defined in (3) and also converted from individual/rotating pitch commands to non-rotating pitch commands via $p = T(\theta)p_{nr}$. In a similar fashion for the outputs, we obtain

$$
\begin{aligned}
\begin{bmatrix} \Omega_g \\ b_{rnr} \\ \beta_{rnr} \end{bmatrix} &= \begin{bmatrix} I & 0 & 0 \\ 0 & T(\theta)^{-1} & 0 \\ 0 & 0 & T(\theta)^{-1} \end{bmatrix} \begin{bmatrix} C_g(\theta) \\ C_b(\theta) \\ C_r(\theta) \end{bmatrix} M(\theta)\hat{x} \\
&\quad + \begin{bmatrix} I & 0 & 0 \\ 0 & T(\theta)^{-1} & 0 \\ 0 & 0 & T(\theta)^{-1} \end{bmatrix} \begin{bmatrix} D_{gsh}(\theta) & D_{gp}(\theta) \\ D_{bsh}(\theta) & D_{bp}(\theta) \\ D_{rsh}(\theta) & D_{rp}(\theta) \end{bmatrix} \begin{matrix} M_{m2s} & 0 & \mathrm{w}_{mbc} \\ 0 & T(\theta) & p_{nr} \end{matrix} \\
\begin{bmatrix} \Omega_g \\ b_{rnr} \\ \beta_{rnr} \end{bmatrix} &= \begin{bmatrix} C_{gMBC}(\theta) \\ C_{bMBC}(\theta) \\ C_{rMBC}(\theta) \end{bmatrix} \hat{x} + \begin{bmatrix} D_{gwMBC}(\theta) & D_{gbMBC}(\theta) \\ D_{bwMBC}(\theta) & D_{bpMBC}(\theta) \\ D_{rwMBC}(\theta) & D_{rpMBC}(\theta) \end{bmatrix} \begin{matrix} \mathrm{w}_{mbc} \\ p_{nr} \end{matrix} \;\; .
\end{aligned}
\qquad \text{(A19)}
$$

An average MBC state-space system is obtained from the complete set of linearizations in the same manner as for the non-MBC case, e.g.,

$$
A_{MBC} = \frac{1}{N}\sum_{i=0}^{N} A_{MBC}(\theta_i). \qquad \text{(A20)}
$$

# B CART3 Controller Design

Time delay is modeled in the most straight forward fashion in discrete time so the starting point for design is conversion of the models in previous sections to discrete time. We use a zero-order hold equivalent (Franklin et al. [27]) and take the liberty of using the same variable names as in the continuous time realization. Then, the controllers are designed by first augmenting the discrete-time, linear model with delays matching the desired preview time so that the time span between the measurement of wind and its arrival at the turbine is incorporated into the model. The model is further augmented so that the closed loop has the desired asymptotic properties with respect to the blade-root bending moments and rotor speed. Plant outputs are selected for performance objectives as required for the standard $\mathcal{H}_\infty$ framework for use with the robust control toolbox in Matlab®. The following sections briefly document the construction of the augmented, generalized plant and its weighted version for $\mathcal{H}_\infty$ design.

## B1 CART3 Non-MBC Preview Controller

Assume that the continuous-time state-space system from the previous section has been converted to discrete time to obtain

$$\begin{aligned} x(k+1) &= Ax(k) + [B_w \; B_p] \begin{matrix} \mathrm{w}_t(k) \\ p(k) \end{matrix} \\ \begin{bmatrix} \Omega_g(k) \\ b_r(k) \\ \beta_r(k) \end{bmatrix} &= \begin{bmatrix} C_g \\ C_b \\ C_r \end{bmatrix} x(k) + \begin{bmatrix} D_{gw} & D_{gp} \\ D_{bw} & D_{bp} \\ D_{rw} & D_{rp} \end{bmatrix} \begin{matrix} \mathrm{w}_t(k) \\ p(k) \end{matrix} , \end{aligned} \tag{B1}$$

where the wind at the turbine $w_t(k)$ is either $w(k)$ or $w_n r(k)$ depending on whether or not the non-MBC/rotating or MBC/non-rotating model is being used. The first step in preview control design is to augment this state-space model with delay chains to incorporate, as part of the turbine model itself, the time span between measurement of wind w and its arrival at the turbine $\mathrm{w}_t$. Say, for example, the amount of preview is three samples, then a state-space realization of this delay is

$$\begin{aligned} x_{wi}(k+1) &= \begin{bmatrix} 0 & 0 & 0 \\ 1 & 0 & 0 \\ 0 & 1 & 0 \end{bmatrix} x_{wi}(k) + \begin{bmatrix} 1 \\ 0 \\ 0 \end{bmatrix} \mathrm{w}_i(k) \\ \mathrm{w}_{ti}(k) &= [0 \; 0 \; 1] \; x_{wi}(k), \end{aligned} \tag{B2}$$

where the measured wind is $w(k)$ and we use one delay chain per measurement/blade ($i = 1, 2, 3$). When these realizations are put in parallel, a composite system with state $x_W^T = [x_{w1}^T, x_{w2}^T, x_{w3}^T]$ is denoted as

$$\begin{aligned} x_W(k+1) &= A_D \; x_W(k) + B_D \; \mathrm{w}(k) \\ \mathrm{w}_t(k) &= C_D \; x_W(k). \end{aligned} \tag{B3}$$

Now, assuming the wind does not change en route to the turbine, an accurate model which includes the delay between measurement and arrival is

$$\begin{array}{rcl} \begin{bmatrix} x(k+1) \\ x_W(k+1) \end{bmatrix} & = & \begin{bmatrix} A & B_w C_D \\ 0 & A_D \end{bmatrix} \begin{bmatrix} x(k) \\ x_W(k) \end{bmatrix} + \begin{bmatrix} 0 & B_p \\ B_D & 0 \end{bmatrix} \begin{bmatrix} \mathrm{w}(k) \\ p(k) \end{bmatrix} \\ \begin{bmatrix} \Omega_g(k) \\ b_r(k) \\ \beta_r(k) \\ \mathrm{w}(k) \end{bmatrix} & = & \begin{bmatrix} C_g & D_{gw} C_D \\ C_b & D_{bw} C_D \\ C_r & D_{rw} C_D \\ 0 & 0 \end{bmatrix} \begin{bmatrix} x(k) \\ x_W(k) \end{bmatrix} + \begin{bmatrix} 0 & D_{gp} \\ 0 & D_{bp} \\ 0 & D_{rp} \\ I & 0 \end{bmatrix} \begin{bmatrix} \mathrm{w}(k) \\ p(k) \end{bmatrix}. \end{array} \tag{B4}$$

Note that the vector of wind measurements $\mathrm{w}(k)$ have been fed through as an additional system output. This is done because the preview controller has access to this vector as a system measurement and it is essentially treated the same as the other feedback signals in the $\mathcal{H}_\infty$ design process.

It is desired to have integral control on generator speed error and rejection of $1P$ variations in the blade-root bending moments. So, the average model is augmented with an integral/accumulator of perturbations $\Omega_g(k)$ in generator speed

$$\begin{array}{rcl} x_s(k+1) & = & x_s(k) + \Omega_g(k) \\ \Omega_{gs}(k) & = & x_s(k), \end{array} \tag{B5}$$

and also with second-order dynamics that oscillate at the $1P$ frequency $\omega_{1p}$. A realization of a $1P$ oscillator is

$$\begin{array}{rcl} \dot{x}_{1p} & = & \begin{bmatrix} 0 & -\omega_{1p} \\ \omega_{1p} & 0 \end{bmatrix} x_{1p} + \begin{bmatrix} 0 \\ 1 \end{bmatrix} u \\ \begin{bmatrix} ys_{1p} \\ yc_{1p} \end{bmatrix} & = & \begin{bmatrix} 1 & 0 \\ 0 & 1 \end{bmatrix} x_{1p}. \end{array} \tag{B6}$$

Both states of the $1P$ dynamics are made available as outputs; the controller will have access to both, but the $ys_{1p}$ output will be made part of the cost. Denote the discrete-time, parallel combination of three of these systems as

$$\begin{array}{rcl} x_{1P}(k+1) & = & A_{1p} x_{1P}(k) + B_{1p}\, b_r(k) \\ \begin{bmatrix} m_{rs}(k) \\ m_{rc}(k) \end{bmatrix} & = & \begin{bmatrix} C_{1ps} \\ C_{1pc} \end{bmatrix} x_{1P}(k), \end{array} \tag{B7}$$

where the input vector $b_r(k)$ is the turbine root bending moments and $m_{rs}$ and $m_{rc}$ hold the $ys_{1p}$ and $yc_{1p}$ outputs, respectively, for the three parallel systems. Now, with these new outputs and additional dynamics, the augmented turbine model is given by

$$\begin{bmatrix} x(k+1) \\ x_W(k+1) \\ x_s(k+1) \\ x_{1P}(k+1) \end{bmatrix} = \begin{bmatrix} A & B_w C_D & 0 & 0 \\ 0 & A_D & 0 & 0 \\ C_g & D_{gw} C_D & 1 & 0 \\ B_{1p}\ C_b & B_{1p}\ D_{bw} C_D & 0 & A_{1p} \end{bmatrix} \begin{bmatrix} x(k) \\ x_W(k) \\ x_s(k) \\ x_{1P}(k) \end{bmatrix} + \begin{bmatrix} 0 & B_p \\ B_D & 0 \\ 0 & D_{gp} \\ 0 & B_{1p}\ D_{bp} \end{bmatrix} \begin{matrix} \mathrm{w}(k) \\ p(k) \end{matrix} \quad \text{(B8)}$$

$$\begin{bmatrix} \Omega_g(k) \\ \Omega_{gs}(k) \\ b_r(k) \\ m_{rs}(k) \\ m_{rc}(k) \\ \beta_r(k) \\ \mathrm{w}(k) \end{bmatrix} = \begin{bmatrix} C_g & D_{gw} C_D & 0 & 0 \\ 0 & 0 & 1 & 0 \\ C_b & D_{bw} C_D & 0 & 0 \\ 0 & 0 & 0 & C_{1ps} \\ 0 & 0 & 0 & C_{1pc} \\ C_r & D_{rw} C_D & 0 & 0 \\ 0 & 0 & 0 & 0 \end{bmatrix} \begin{bmatrix} x(k) \\ x_W(k) \\ x_s(k) \\ x_{1P}(k) \end{bmatrix} + \begin{bmatrix} 0 & D_{gp} \\ 0 & 0 \\ 0 & D_{bp} \\ 0 & 0 \\ 0 & 0 \\ 0 & D_{rp} \\ I & 0 \end{bmatrix} \begin{matrix} \mathrm{w}(k) \\ p(k) \end{matrix} .$$

Finally, for the sake of completeness, we document the final two steps in the process of generalizing the average model for $\mathcal{H}_\infty$ design. The plant outputs (with the exception of $m_{rc}$ and w) are duplicated and serve as the cost objective, and the original set of outputs (with the exception of the pitch rate $\beta_r$) are made available for feedback to the controller.

All the performance outputs are weighted by additional scalar factors except for the generator speed output which requires additional handling. Dynamics are added to this output to emphasize the drivetrain resonance at frequency $\Omega_{dt}$ and thereby assure sufficient damping of this mode. We use a dynamic weight given by

$$\mathrm{w}_{dt}(s) = \frac{s/(0.2 \cdot 2\pi) + 1}{(s/\Omega_{dt})^2 + s/\Omega_{dt}/5 + 1}, \quad \text{(B9)}$$

that has gain increasing from unity at 0.2 Hz with a 14 dB peak (a Q factor of 5) at the drivetrain resonance and then a 20dB/dec (decibels per decade) roll off thereafter. Denote a discrete-time realization of this weighting function by

$$\begin{aligned} x_{dt}(k+1) &= A_{dt} x_{dt}(k) + B_{dt} \Omega_g(k) \\ \Omega_{gw}(k) &= C_{dt} x_{dt}(k), \end{aligned} \quad \text{(B10)}$$

and let $[K_{dt}, K_s, K_m, K_{pr}]$ denote additional scalar weights for the generator speed, integral of generator speed, and pitch rate, respectively. Define the vector of performance outputs as $y_p$ and the vector of feedback outputs as $y_f$. Then, the final form of the generalized turbine model is

$$\begin{bmatrix} x(k+1) \\ x_W(k+1) \\ x_s(k+1) \\ x_{1P}(k+1) \\ x_{dt}(k+1) \end{bmatrix} = \begin{bmatrix} A & B_w C_D & 0 & 0 & 0 \\ 0 & A_D & 0 & 0 & 0 \\ C_g & D_{gw} C_D & 1 & 0 & 0 \\ B_{1p} C_b & B_{1p} D_{bw} C_D & 0 & A_{1p} & 0 \\ B_{dt} C_g & B_{dt} D_{gw} C_D & 0 & 0 & A_{dt} \end{bmatrix} \begin{bmatrix} x(k) \\ x_W(k) \\ x_s(k) \\ x_{1P}(k) \\ x_{dt}(k) \end{bmatrix} + \begin{bmatrix} 0 & B_p \\ B_D & 0 \\ 0 & D_{gp} \\ 0 & B_{1p} D_{bp} \\ 0 & B_{dt} D_{gp} \end{bmatrix} \begin{matrix} \mathrm{w}(k) \\ p(k) \end{matrix}$$

(B11)

$$\begin{matrix} y_p(k) \\ y_f(k) \end{matrix} \triangleq \begin{bmatrix} \begin{bmatrix} \Omega_{gw}(k) \\ \Omega_{gs}(k) \\ b_r(k) \\ m_{rs}(k) \\ \beta_r(k) \end{bmatrix} \\ \begin{bmatrix} \Omega_g(k) \\ \Omega_{gs}(k) \\ b_r(k) \\ m_{rs}(k) \\ m_{rc}(k) \\ \mathrm{w}(k) \end{bmatrix} \end{bmatrix} = \begin{bmatrix} 0 & 0 & 0 & 0 & K_{dt} C_{dt} \\ 0 & 0 & K_s & 0 & 0 \\ K_m C_b & K_m D_{bw} C_D & 0 & 0 & 0 \\ 0 & 0 & 0 & C_{1ps} & 0 \\ K_{pr} C_r & K_{pr} D_{rw} C_D & 0 & 0 & 0 \\ C_g & D_{gw} C_D & 0 & 0 & 0 \\ 0 & 0 & 1 & 0 & 0 \\ C_b & D_{bw} C_D & 0 & 0 & 0 \\ 0 & 0 & 0 & C_{1ps} & 0 \\ 0 & 0 & 0 & C_{1pc} & 0 \\ 0 & 0 & 0 & 0 & 0 \end{bmatrix} \begin{bmatrix} x(k) \\ x_W(k) \\ x_s(k) \\ x_{1P}(k) \\ x_{dt}(k) \end{bmatrix} + \begin{bmatrix} 0 & 0 \\ 0 & 0 \\ 0 & K_m D_{bp} \\ 0 & 0 \\ 0 & K_{pr} D_{rp} \\ 0 & D_{gp} \\ 0 & 0 \\ 0 & D_{bp} \\ 0 & 0 \\ 0 & 0 \\ I & 0 \end{bmatrix} \begin{matrix} \mathrm{w}(k) \\ p(k) \end{matrix} .$$

$\mathcal{H}_\infty$ optimization finds a dynamic, stabilizing, output-feedback controller

$$p(k) = G \cdot y_f(k), \tag{B12}$$

that minimizes

$$J(G) = \frac{\sum_{k=0}^{\infty} y_p(k)^T y_p(k)}{\sum_{k=0}^{\infty} \mathrm{w}(k)^T \mathrm{w}(k)}. \tag{B13}$$

It can be shown that this is equivalent to minimizing the peak over all frequencies of the maximum singular value of the closed-loop transfer function from w to $y_p$ (Francis [28]). We use the robust control toolbox in Matlab® to find a near optimum controller for two different values of the pitch-rate weight $K_{pr}$ and thereby get controllers that have different rms pitch rates.

Figure B1 shows the open-loop plant and weighted performance outputs. The augmented responses show that we require asymptotic rejection of DC speed at the generator (top plot) and $1P$ bending moments in the blade-root flap (center plot); the gain in the performance/cost at these frequencies is infinite. The lower plot shows that the weight applied to pitch is biased towards high frequencies and dominates (in terms of magnitude) the performance outputs. The blue "Pr W1" and red "Pr W2" weights result in rms pitch rates of about 7 deg/sec and 11 deg/sec respectively. The response with respect to the other blade local wind inputs is the same; although it is not apparent without seeing the response of blade 2 to disturbances at blade 1, the wind-to-bending moment responses are largely uncoupled.

## B2 CART3 MBC Preview Controller

The procedure for design of the MBC preview controller is nearly identical to that used in the non-MBC case, except of course, that the starting point is the linearized, MBC turbine model (A18) and (A19). There are two additional significant caveats. The first is in implementation (see Figure 19(b)) where all the signals going into the controller need (if they are not already) to be transformed to non-rotating coordinates via $T^{-1}(\theta)$, but the outputs of the controller need to be transformed back to rotating coordinates with $T(\theta)$. The second is that in the non-rotating frame, $1P$ variations appear as DC amplitudes in the cosine and sine components. The upshot being that in order to have asymptotic rejection of $1P$ bending moments, we only need to augment the system with integrators on the cosine and sine components as compared with the use of three second-order oscillating systems on the individual bending moments as in the non-MBC case. The use of MBC coordinates affords another significant advantage in this regard in that the rejection of $1P$ variations is accomplished independent of rotor speed. In the non-MBC case, the plant was augmented with dynamics which only oscillate at exactly $\omega_{1p}$ and therefore only provide asymptotic rejection at that frequency. When rotor speed is not at the expected $\omega_{1p}$, then the ability of the non-MBC controller to attenuate $1P$ variation is diminished. Use of the MBC transform, which determines the amplitude (and phase) of the $1P$ variation spatially as a function of rotor position instead of speed, circumvents this problem.

Again, the discrete-time, average, MBC turbine (+actuator) model is augmented with delays equal to the desired preview. However, in this case, the input to the delays is a measure of the non-rotating (MBC transformed) components of the wind in front of the turbine. The turbine model is also augmented with integrators on the cosine and sine components of blade-root bending moment, and the same performance weighting on the generator speed output (this output is in the non-rotating frame so it is the same in MBC and non-MBC cases).

We spare the reader from another derivation that would be nearly identical to the one presented for generalizing the non-MBC turbine. Instead, we simply state that the generalized MBC turbine model can be obtained from (B11) by replacing non-MBC matrices with their MBC counterparts, removing the $m_{rc}$ output, and replacing the state-space realization $\{A_{1p}, B_{1p}, C_{1p}\}$ for three parallel, second-order $1P$ oscillators with the simpler realization $\{I_{2x2}, I_{2x2}, I_{2x2}\}$ for two parallel accumulators. This serves to augment the MBC model with accumulators on perturbations in the cosine and sine components of the non-rotating bending moment.

Figure B2 shows the plant open loop and weighted performance outputs except for pitch rate which is displayed in Figure B3. Unlike the non-MBC plot in Figure B1 which shows the response from only one input, we show the response from all MBC inputs to all outputs. This serves to illustrate that the collective channel is significantly different than the vertical and horizontal channels and to show that the system is to a large extent diagonal. That is, the collective output is very insensitive to vertical and horizontal perturbations (and vice-versa); the vertical and horizontal outputs are uncoupled except at frequencies greater than 1 Hz. The same observations with respect to coupling can be made upon viewing the MBC pitch model response in Figure B3. As was the case for the non-MBC design, the blue "W1" and red "W2" weights result in rms pitch rates of about 7 deg/sec and 11 deg/sec respectively.

## B3 CART3 Non-Preview Baseline Controllers

We conclude with bode plots of the non-preview controller loops shown in Fig. B4. These are very conservative PI controllers designed with bandwidths that hopefully minimize the amount of bending moment generated during speed regulation and also prevent the vertical and horizontal MBC loops from coupling.

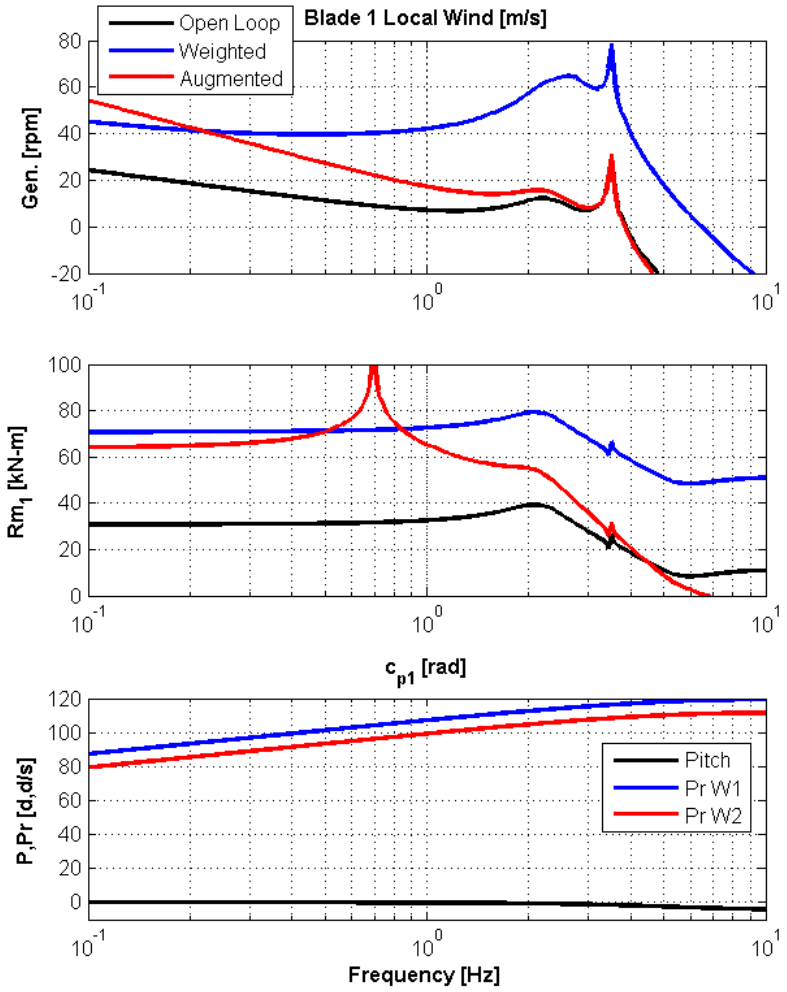


Figure B1. Non-MBC Performance Output Weighting: in all cases, larger response /more weight implies better attenuation in closed loop; top two plots— response to blade 1 local wind disturbances; top— weighting on the generator speed output; center— weighting on blade-root bending moments; bottom— weighting on the pitch actuator outputs.

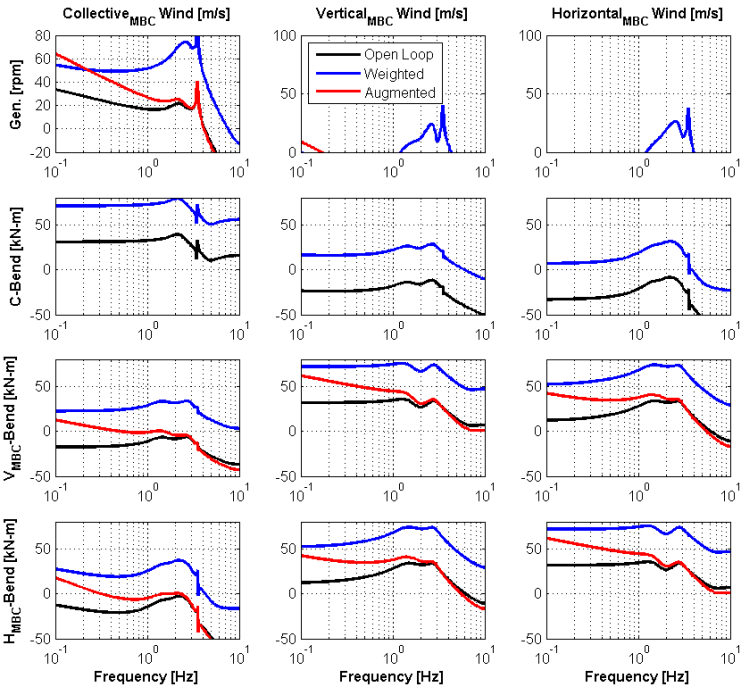


Figure B2. MBC Performance Output Weighting: in all cases, larger response/more weight implies better attenuation in closed loop; top row— generator speed weighting; lower three rows— MBC collective, vertical, and horizontal bending moment component weighting respectively.

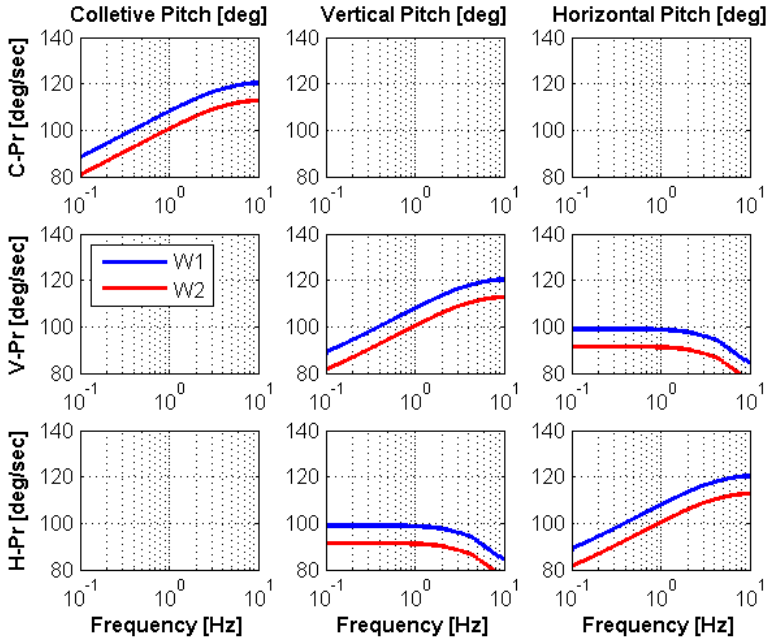


Figure B3. pitch-rate weighting: in all cases, larger response/more weight implies less pitch in closed loop.

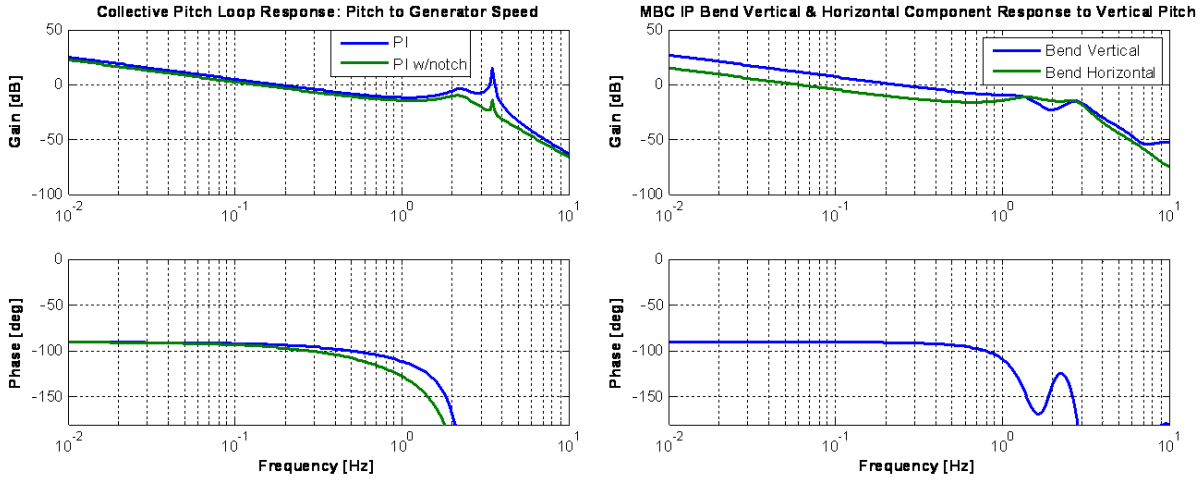


Figure B4. Baseline loop responses: (a) Collective pitch to generator speed; (b) vertical-to-vertical and horizontal-to-horizontal loops.

# REPORT DOCUMENTATION PAGE

*Form Approved*
*OMB No. 0704-0188*



**PLEASE DO NOT RETURN YOUR FORM TO THE ABOVE ORGANIZATION.**

| 1. REPORT DATE *(DD-MM-YYYY)* | 2. REPORT TYPE | 3. DATES COVERED *(From - To)* |
|---|---|---|
| December 2010 | subconract report | Jan. 2009 - Jan. 2010 |

**4. TITLE AND SUBTITLE**
Feasibility Studies on Disturbance Feedforward Techniques to Improve Wind Turbine Load Mitigation Performance

**5a. CONTRACT NUMBER**
DE-AC36-08GO28308

**5b. GRANT NUMBER**

**5c. PROGRAM ELEMENT NUMBER**

**6. AUTHOR(S)**
J.H. Laks, F. Dunne, and L.Y. Pao

**5d. PROJECT NUMBER**
NREL/SR-5000-48598

**5e. TASK NUMBER**
WE103131

**5f. WORK UNIT NUMBER**

**7. PERFORMING ORGANIZATION NAME(S) AND ADDRESS(ES)**
University of Colorado
Boulder, Colorado

**8. PERFORMING ORGANIZATION REPORT NUMBER**
XEE-9-99404-01

**9. SPONSORING/MONITORING AGENCY NAME(S) AND ADDRESS(ES)**
National Renewable Energy Laboratory
1617 Cole Blvd.
Golden, CO 80401-3393

**10. SPONSOR/MONITOR'S ACRONYM(S)**
NREL

**11. SPONSORING/MONITORING AGENCY REPORT NUMBER**
NREL/SR-5000-48598

**12. DISTRIBUTION AVAILABILITY STATEMENT**
National Technical Information Service
U.S. Department of Commerce
5285 Port Royal Road
Springfield, VA 22161

**13. SUPPLEMENTARY NOTES**
NREL Technical Monitor: Alan Wright

**14. ABSTRACT** *(Maximum 200 Words)*
This study investigates disturbance feedforward and preview control to better understand the best possible improvement in load mitigation using advanced wind measurement techniques.

**15. SUBJECT TERMS**
wind turbine control techniques; wind measurement; wind turbine load mitigation; wind energy

| 16. SECURITY CLASSIFICATION OF: | | | 17. LIMITATION OF ABSTRACT | 18. NUMBER OF PAGES | 19a. NAME OF RESPONSIBLE PERSON |
|---|---|---|---|---|---|
| a. REPORT | b. ABSTRACT | c. THIS PAGE | | | 19b. TELEPHONE NUMBER (*Include area code)* |
| Unclassified | Unclassified | Unclassified | UL | | |

**Standard Form 298** (Rev. 8/98)
Prescribed by ANSI Std. Z39.18